Title: Extracellular vesicles alter trophoblast function in pregnancies complicated by COVID-19

One Sentence Summary: Circulating extracellular vesicles are altered by COVID-19 during pregnancy and contribute to placental dysfunction.

Authors: Thea N. Golden[1,2,3*], Sneha Mani[1,2], Rebecca L. Linn[4], Rita Leite[1,2], Natalie A. Trigg[5], Annette Wilson[6], Lauren Anton[1,2], Monica Mainigi[1,2], Colin C. Conine[2,5,7,8,9,10], Brett A. Kaufman[6], Jerome F. Strauss III[1,2], Samuel Parry[1,2], and Rebecca A. Simmons[2,3,9,10]

Affiliations:

[1]Department of Obstetrics and Gynecology, Perelman School of Medicine at the University of Pennsylvania; Philadelphia, USA.

[2]Center for Research on Reproduction and Women's Health, University of Pennsylvania; Philadelphia, USA.

[3]Center for Excellence in Environmental Toxicology, University of Pennsylvania; Philadelphia, USA.

[4]Department of Pathology and Laboratory Medicine, Children's Hospital of Philadelphia; Philadelphia, USA.

[5]Epigenetics Institute, Perelman School of Medicine at the University of Pennsylvania; Philadelphia, USA.

[6]Department of Medicine, University of Pittsburgh; Pittsburgh, USA.

[7]Institute for Regenerative Medicine, Perelman School of Medicine at the University of Pennsylvania; Philadelphia, USA.

[8]Department of Genetics, Perelman School of Medicine at the University of Pennsylvania; Philadelphia, USA.

23 [9]Department of Pediatrics, Perelman School of Medicine at the University of Pennsylvania;
24 Philadelphia, USA.
25 [10]Division of Neonatology, Children's Hospital of Philadelphia, Philadelphia, USA.
26 *Corresponding author. Email: goldent@pennmedicine.upenn.edu

27

28 **Abstract:**

29 Severe acute respiratory syndrome coronavirus 2 (SARS-CoV-2) infection and resulting
30 coronavirus disease (COVID-19) causes placental dysfunction, which increases the risk of
31 adverse pregnancy outcomes. While abnormal placental pathology resulting from COVID-19 is
32 common, direct infection of the placenta is rare. This suggests that pathophysiology associated
33 with maternal COVID-19, rather than direct placental infection, is responsible for placental
34 dysfunction and alteration of the placental transcriptome. We hypothesized that maternal
35 circulating extracellular vesicles (EVs), altered by COVID-19 during pregnancy, contribute to
36 placental dysfunction. To examine this hypothesis, we characterized maternal circulating EVs
37 from pregnancies complicated by COVID-19 and tested their effects on trophoblast cell
38 physiology *in vitro*. We found that the gestational timing of COVID-19 is a major determinant
39 of circulating EV function and cargo. *In vitro* trophoblast exposure to EVs isolated from patients
40 with an active infection at the time of delivery, but not EVs isolated from Controls, altered key
41 trophoblast functions including hormone production and invasion. Thus, circulating EVs from
42 participants with an active infection, both symptomatic and asymptomatic cases, can disrupt vital
43 trophoblast functions. EV cargo differed between participants with COVID-19 and Controls,
44 which may contribute to the disruption of the placental transcriptome and morphology. Our

45 findings show that COVID-19 can have effects throughout pregnancy on circulating EVs and
46 circulating EVs are likely to participate in placental dysfunction induced by COVID-19.
47

48 **INTRODUCTION**

49 Maternal SARS-CoV-2 infection and resulting coronavirus disease (COVID-19) is
50 associated with an increased risk of pregnancy complications including preterm birth,
51 hypertensive disorders of pregnancy, fetal growth restriction, and pregnancy loss (*1, 2*).
52 Placental dysfunction is known to contribute to these complications, and placental pathology,
53 including vasculopathies and inflammation, is frequently reported following an acute or even
54 resolved infection during pregnancy (*3-6*). This suggests COVID-19 has a long-lasting effect on
55 pregnancy by altering placenta function. Despite extensive reports of placental abnormalities
56 following COVID-19, little is known about the underlying mechanisms contributing to placental
57 dysfunction and the related subsequent pregnancy complications. Direct infection of the
58 placenta is rare, which suggests that placental dysfunction is caused by the maternal response to
59 SARS-CoV-2 infection (*6-8*).

60 Circulating extracellular vesicles (EVs) are altered by SARS-CoV-2 infection and
61 contribute to COVID-19-induced organ damage (*9-13*). EVs are a means of cell-to-cell
62 communication resulting from their ability to carry and transfer bioactive cargo that elicits
63 signaling events in recipient cells. Compared to uninfected individuals, EV cargo composition in
64 patients with COVID-19 is significantly different, eliciting downstream systemic effects such as
65 coagulopathy (*14-17*) and inflammation (*10, 11, 14, 18*). For example, tissue factor protein
66 abundance in EVs is increased in COVID-19 and correlates with inflammation and disease

67 severity demonstrating the influence that circulating EVs have on the systemic response to
68 COVID-19, thereby leading to organ dysfunction (*9, 12, 13*).
69 During normal pregnancy, the placenta releases EVs into the maternal circulation (*19,*
70 *20*). Placental-derived EVs promote maternal adaptation to support a healthy pregnancy
71 including a shift in the maternal immune system to a tolerant state and the promotion of
72 angiogenesis (*21, 22*). Placental-derived EVs also affect trophoblast function through autocrine
73 and paracrine signaling. Trophoblasts are a specialized cell type of the placenta that are
74 responsible for invasion into maternal tissue to anchor the placenta, vascular remodeling for
75 adequate placental blood flow, nutrient transport, and hormone production for maternal and fetal
76 signaling. EV signaling impairs normal trophoblast function which is thought to contribute to
77 the placental dysfunction underlying pregnancy complications (*21, 23-26*).
78 Therefore, we hypothesized that COVID-19 alters circulating EV cargo which has a
79 functional consequence in the placenta. Similar to previous studies, we found that COVID-19
80 during pregnancy induced marked placental histologic and transcriptomic changes that were
81 dependent on the gestational timing of maternal SARS-CoV-2 infection. Importantly, we found
82 that COVID-19 altered EV cargo, and trophoblast exposure to these EVs resulted in reduced
83 trophoblast invasion and hormone production.

84 **RESULTS**

85 **Pregnancy outcomes following active and resolved SARS-CoV-2 infection**

86 Participants were enrolled at the time of delivery between July 2020-August 2022.
87 Controls had no known SARS-CoV-2 infection during pregnancy. COVID-19 cases were
88 divided based on the gestational timing of infection and either had a resolved infection that
89 occurred in the 1st, 2nd, or 3rd trimester (R1, R2, R3), or had an active infection at the time of

90 delivery (AI) (Table 1). All patients admitted to the labor and delivery unit underwent PCR
91 testing for SARS-CoV-2 at admission. There were no significant differences in maternal age
92 between groups, but there were significantly more Black participants with an infection in the
93 third trimester (resolved or active) compared to non-infected individuals (Controls) (R3 p=0.046,
94 AI p=0.011). Participants with an infection in the third trimester, resolved or active, also had an
95 earlier gestational age at delivery than Controls (R3 p<0.001, AI p=0.034) (Table 1). Not
96 surprisingly, the AI group, which underwent universal screening for SARS-CoV-2 at admission
97 for delivery, had a higher incidence of asymptomatic infection than those with resolved infection
98 (p<0.0001).

99 Multiple studies have shown that SARS-CoV-2 infection during pregnancy is associated
100 with adverse pregnancy outcomes. However, to date, no study has examined the relationship
101 between the timing of infection and pregnancy complications in a single cohort. Our study is
102 limited by relatively small numbers (n=15-32) in each participant group, but we found that the
103 type of adverse outcome differed depending on the gestational timing of infection. The
104 incidence of gestational hypertension (gHTN) was increased in R1 (p=0.016), whereas
105 spontaneous preterm birth (SPTB) was increased in R2 (p=0.008) compared to Controls.
106 Preeclampsia (PE) and medically indicated preterm birth (MPTB) were increased in R3 and AI
107 compared to Controls (PE: R3 p=0.032, AI p= 0.010, MPTB: R3 p=0.005, AI p=0.010) (Table
108 1). In our cohort, there was no increase in intrauterine growth restriction (IUGR) or intrauterine
109 fetal demise (IUFD) which have been reported in pregnancies complicated by COVID-19 (*27-*
110 *29*).

111 **Placental pathology in COVID-19**

112 Abnormal placental pathology is commonly reported in patients with active and resolved
113 SARS-CoV-2 infections (*3*). However, there has yet to be a comprehensive assessment of
114 placenta morphology following maternal infection at various gestational ages. Similar to
115 previous reports (*3-6, 30, 31*), we found maternal and fetal vascular malperfusion (MVM &
116 FVM) lesions were increased among patients with pregnancies complicated by COVID-19
117 (Table 1). Interestingly, high-grade MVM and perivillous fibrin deposition were increased in
118 participants with a resolved infection that occurred in the second or third trimester, but not the
119 first trimester or with an active infection. This suggests that it takes a substantial amount of time
120 for the placenta to recover from the impact of COVID-19. Alternatively, it is possible that the
121 first trimester placenta was more resilient. The lack of high-grade MVM and perivillous fibrin
122 deposition in placenta collected from participants with an active infection suggests these lesions
123 may take weeks to manifest.

124 **Timing of COVID-19 impacts the placental transcriptome**

125 To gain insight into potential novel pathways that might be affected by COVID-19 during
126 pregnancy, we performed RNA-seq on the placental transcriptome using biopsies from placenta
127 collected at delivery in COVID-19 cases and controls. Not surprisingly, active infection was
128 associated with significant differences in gene expression in the placenta. There were 72
129 upregulated genes and 384 downregulated genes in AI compared to Control placentas. (Figure 1,
130 Supplemental Table 1). Gene expression was also altered in recovered infections, but the
131 magnitude of change was smaller; 28, 2, and 56 differentially expressed genes (DEGs)
132 comparing R1, R2, and R3 to Controls, respectively. It's worth noting that in each of the 4
133 groups, there was differential expression of genes that regulate mitochondria activity, which
134 implies a common dysfunctional pathway resulting from COVID-19.

135 In addition, several other genes were differentially expressed in one or more COVID-19
136 groups. There were several transcripts that were increased in placenta from R1 and AI groups
137 compared to Controls. Several of these genes regulate fibrosis (*RORB*, *FN1*, *IGFB6*, *MMP12*,
138 and *AC027288.3*) (*32-36*) suggesting that this pathway plays an important role in placenta
139 pathology in COVID-19. Moreover, MMP12 regulates spiral artery remodeling and reduced
140 MMP12 activity contributes to the development of preeclampsia (*37*). Similarly, increased
141 expression of *FN1* slice variants containing Extra Domain A promotes inflammation via Toll-
142 like receptor 4 (TLR4) activation (*38, 39*) and is associated with an increased risk of
143 preeclampsia (*32, 38, 39*). Dysregulation of these pathways may contribute to the pathogenesis
144 of preeclampsia in pregnant individuals with COVID-19. Finally, *GREB1* was upregulated in R1
145 and AI placenta compared to Controls. GREB1 interacts with the progesterone (P4) receptor to
146 regulate P4 responsive genes (*40, 41*) and GREB1 promotes maternal tissue remodeling (*40*).
147 Several of the downregulated genes in AI compared to Controls were also
148 downregulated in R3 placenta compared to Controls (*PRELP*, *MEG9*, *VSTM4*, *CLIC2*, *C7*, and
149 *CNN1*). Interestingly, *CNN1*, which encodes calponin, is expressed by smooth muscle cells and
150 expression changes are associated with spiral artery remodeling (*42, 43*). Further, SARS-CoV-2
151 infection is known to disrupt complement pathways (*44*) and the gene encoding complement C7
152 was downregulated in R3 and AI placenta compared to Controls. The complement system plays
153 a dual role in pregnancy in that it protects the placenta from pathogen infection and participates
154 in spiral artery remodeling (*45*). While the effect of decreased *C7* in the placenta is unknown, it
155 may indicate that an imbalance in the complement system contributes to placental pathology
156 observed in R3 and AI placentas. *STAT4*, which encodes the signal transducer and activator of
157 transcription 4, is a key activator of immune regulating genes and was upregulated in R3 and AI

158 placentas compared to Controls. STAT4 mediated pathways are disrupted in preeclampsia and
159 circulating levels are elevated in patients with preeclampsia (*46, 47*). This differential gene
160 expression was only seen in the placenta if the maternal infection was active or recently resolved,
161 suggesting a long period of time is necessary to attenuate these pathways.

162 Statistically significant disruptions in canonical pathways, as determined by Ingenuity
163 Pathway Analysis (IPA), include inflammation and fibrosis in the placentas from R1, R3, and AI
164 compared to Controls (Supplemental Table 2). This unbiased approach based on differential
165 gene expression supported our placental histopathology findings of inflammation and fibrosis in
166 these placentas. Thus, despite the long period of time following the resolution of maternal
167 SARS-CoV-2 infection, genes that regulate fibrosis and inflammation were altered, and
168 pathological evidence of fibrosis and inflammation were apparent in the placenta regardless of
169 the timing of infection.

170 We also used IPA to predict transcriptional regulators of genes differentially expressed in
171 the placenta from pregnancies complicated by COVID-19. Interestingly, genes that encode for
172 growth factors (IGF1, *IGF2*, *FGF3, FGF19, TGFB1*), immune-regulating proteins (*JUN, TNF,*
173 *IL1B, IL13, IL6, IL10, IL4, IFNG*) and hormone-regulating proteins (*PRLH, LEPR, ESR1, and*
174 *PGR*) were the top predicted transcriptional regulators (Supplemental Table 3).

175 **Sustained effects on circulating EVs following COVID-19 in early pregnancy**

176 As discussed above, SARS-CoV-2 rarely infects the placenta, implying a distal signal.
177 We hypothesized that maternal circulating EVs play a role in mediating placental dysfunction
178 associated with COVID-19. Therefore, we characterized EVs isolated from maternal plasma
179 collected at delivery to determine if COVID-19 altered the EV profile. We isolated large (LEV)
180 and small (SEV) EVs as they carry distinct cargo with distinct functional effects. We confirmed

181 the presence of large and small EVs in isolated particles by electron microscopy (Supplemental
182 Figure 1A). Large and small EVs had the expected size distribution of EVs (Supplemental
183 Figure 1B) and abundant expression of the EV-related tetraspanin CD9 (Supplemental Figure
184 1C).

185 EV characteristics, including concentration and size distribution, revealed long-lasting
186 alterations in patients with a resolved infection. The diameter of small EVs was significantly
187 increased in resolved infections compared to Controls (108.7nm vs. 117.2nm, p=0.023).
188 However, the difference in concentration was not significant (2.15×10^8 vs. 1.56×10^8 EVs/uL
189 plasma, p=0.074). When resolved infections were categorized by timing during gestation, we
190 found that small EVs isolated from R2 participants had an increased diameter and reduced
191 concentration, but small EVs isolated from R1 and R3 participants were not different from
192 Controls (Figure 2 D&E). The diameter of large EVs isolated from R2 patients was decreased
193 but there was no change in their number (Figure 2 A&B). COVID-19 in the second trimester was
194 uniquely associated with alterations in circulating EV concentration and size at the time of
195 delivery.

196 **Altered cell of origin of EVs in patients with COVID-19 in early pregnancy**

197 Characterizing the source of circulating EVs provides biological information about the
198 tissue and cell-type of origin and its functional state. We used flow cytometry to detect cell-
199 specific vesicle membrane protein expression and identified the relative contribution of each EV
200 tissue-cellular source. We identified EVs that originated from maternal endothelial cells (CD31+
201 CD34-), fetal endothelial cells (CD31+ CD34+), platelets (CD41a+), immune cells (CD45+), and
202 trophoblasts (PLAP+) (Figure 2 C&F).

203 Trophoblast-derived PLAP+ EVs comprised the largest proportion of circulating large
204 EVs (Figure 2C). The percentage of PLAP+ EVs was increased in the circulation of R2
205 compared to Controls suggesting the placenta secreted more large EVs into circulation.
206 Interestingly, we found a subset of endothelial-derived EVs that also express CD34, suggesting
207 that these EVs originated from fetal endothelial cells (*48*). Fetal endothelial cell-derived large
208 EVs (CD34+ CD31+) were also elevated in R1 and R2 compared to Controls. The percentage of
209 small EVs from the placenta was not altered by COVID-19 (Figure 2F). In fact, there was no
210 difference in the percentage of small EVs from any cell type measured. This suggests that
211 placenta-derived large, but not small EVs, were altered by COVID-19 in early pregnancy.

212 **Circulating EVs from COVID-19 pregnant patients alter trophoblast function *in vitro***

213 The placenta is made up of three main functional cell types; 1) syncytiotrophoblast cells,
214 which are responsible for nutrient transport and hormone production; 2) cytotrophoblast cells,
215 the replicating precursors of the syncytiotrophoblast; and 3) extravillous trophoblasts (EVT),
216 which invade deep into the uterus to anchor the placenta and enable blood and nutrient flow to
217 the fetus. EV signaling is known to influence trophoblast function (*49*). Therefore, we tested the
218 capacity of circulating EVs isolated from participants with an active infection or Controls to alter
219 the function of trophoblast cell types. We focused our *in vitro* experiments on EVs isolated from
220 participants with an active infection compared to Controls because the changes in placental
221 pathology and transcriptome were the greatest in AI cases compared to Controls.

222 To assess the effect of AI EVs on EVT function, we used primary EVTs isolated from
223 first-trimester placenta and quantified EVT invasion through a collagen gel. EVT invasion,
224 which is vital for anchoring the placenta to the uterus and the remodeling of maternal uterine
225 arteries providing blood to the villous trophoblasts, was significantly reduced by exposure to AI

226 EVs compared to Control EVs (Figure 3A). Inadequate invasion and failure to completely
227 remodel maternal arteries increases the risk of preeclampsia, intrauterine growth restriction, and
228 fetal loss (*50, 51*).

229 To study syncytiotrophoblasts, we used the BeWo choriocarinoma cell line that is
230 commonly used to study this trophoblast lineage. After the addition of forskolin, BeWo cells
231 syncytialize forming cells that mimic the syncytiotrophoblast, including the production of
232 placental hormones (hCG and progesterone). Syncytiotrophoblast hormone production is
233 essential for the maintenance of pregnancy. The ratio of hCG to progesterone in the media of
234 syncytialized BeWo cells was significantly reduced following exposure to AI EVs compared to
235 Control EVs (Figure 3B). A reduction in the ratio of hCG to progesterone indicates that specific
236 pathways related to steroid hormone production were disrupted. These findings demonstrate that
237 EVs from the circulation of a pregnant individual with an active infection disrupt major
238 trophoblast functions including invasion and hormone production, which may have profound
239 effects on pregnancy maintenance.

240 To identify novel pathways that may contribute to trophoblast dysfunction, we analyzed
241 the BeWo transcriptome following EV exposure. AI EVs significantly altered gene expression
242 in BeWo cells compared to Control EVs. Multiple genes were dysregulated including genes that
243 encode for long non-coding RNA genes and histone proteins (Figure 3C). This suggests that
244 DNA packaging and transcription is disrupted in trophoblasts exposed to AI EVs compared to
245 Control EVs. Consistent with this, Biological Processes, determined by GO analysis, and top
246 canonical pathways, identified by IPA, were related to cellular transcription and DNA repair
247 (Figure 3D and Supplemental Table 4). The pathways disrupted by AI EVs suggest a
248 generalized effect on trophoblast gene expression that led to disrupted hormone production.

249 **Increased mtDNA content in LEVs following COVID-19 in early pregnancy**

250 Analysis of the placental transcriptome following COVID-19 identified differentially
251 expressed genes indicative of mitochondrial dysfunction (Table 2). To determine if circulating
252 EVs were enriched in mitochondrial cargo, we measured mitochondrial DNA (mtDNA) content
253 (Figure 4A &C) and found that mtDNA was more abundant in large compared to small EVs. In
254 contrast, nuclear DNA was not consistently measurable in all samples. Additionally, the
255 abundance of mtDNA in large, but not small EVs, inversely correlated with the gestational
256 timing of COVID-19 (Figure 4 B&D). The increase in mtDNA released in large EVs following
257 COVID-19 during early pregnancy suggests that the mitochondrial function of cells producing
258 large EVs was persistently disrupted.

259 **COVID-19 during pregnancy alters EV RNA cargo**

260 EVs contain small and larger (mRNAs) and long noncoding RNAs, however, small
261 RNAs are the most commonly studied EV cargo (*52*). mRNAs encapsulated within EVs are
262 transferred to recipient cells and translated into proteins, altering the behavior of the recipient
263 cells (*53-56*). Therefore, we profiled the mRNA content of circulating EVs to determine if there
264 were differences dependent on the gestational timing of COVID-19. We sequenced an average
265 of 2,946 gene associated transcripts in large EVs and 1,947 in small EVs.

266 The most abundant mRNA transcripts in EVs were common to all groups. However, we
267 also identified transcripts that were either uniquely expressed in COVID-19 groups (i.e. absent in
268 Controls), or uniquely expressed in Controls, and absent in one or more COVID-19 groups.
269 Multiple transcripts were uniquely expressed in large EVs from the COVID-19 groups including
270 *YY1AP1*, *MOSPDI, RYBP*, and *H1-4* (Table 2). The proteins encoded by these mRNAs are
271 related to transcription, except for *HI-4* which has an unknown cellular function. In small EVs,

272 *MYL4*, *C18orf32*, *CAPG*, and *CTSS* transcripts were uniquely present in EVs isolated from
273 COVID-19 groups (Table 2). These transcripts encode a motor (*MYL4* (myosin light chain 4))
274 and immune (*C18orf32* (Putative NF-Kappa-B-Activating Protein 200), *CAPG* (macrophage
275 capping protein), and *CTSS* (cathepsin S)) proteins. This suggests that COVID-19 alters
276 immune-related small EV cargo. Many other transcripts were uniquely detected in EVs isolated
277 from individual COVID-19 groups (Table 2). The unique transcriptome suggests that COVID-
278 19 increased expression of these genes making their transcripts more available for EV packaging
279 or increased specific transcript loading into EVs.

280 There were several interesting transcripts that were only present in large EVs from
281 Controls, including APBA3, MTSS, FCF1, PSG2, LOC100128233, PHOSPHO2, and THOC3
282 (Figure 5A). These transcripts encode proteins involved in various cellular functions, including
283 signal transduction, transcription, and proliferation. In contrast, only a few transcripts were
284 unique to Controls in small EVs. These included PYCR2, SCGB1C1, and CD300L4 (Figure
285 5B). PYCR2 encodes a cellular metabolism protein; CD300L4 encodes an immune-regulating
286 protein. The protein function of SCGB1C1 is unknown. Numerous other transcripts were
287 abundant in Controls but absent in individual COVID-19 groups. If present in the other COVID-
288 19 groups, their expression was decreased compared to Controls (Figure 5).

289 Transcripts carried by EVs reflect the activity of the secreting cell. While the individual
290 transcripts identified in EVs differ, their cellular functions often overlapped (Table 2, Figure 5).
291 For example, large and small EVs isolated from R2 carried transcripts that regulate cell
292 signaling, gene expression, immune regulation, and metabolism. Additional pathways include
293 proliferation, apoptosis, invasion, ubiquitination, platelet function, and vesicle formation.

294 Many transcripts identified in EVs are abundant in trophoblast cells and have been
295 previously reported to increase with gestation. Interestingly, *THOC3* mRNA, encoded by a
296 highly expressed gene in trophoblast cells, was abundant in Control large EVs but was low or
297 absent in the COVID-19 groups. In addition, large EVs carried a different highly expressed
298 trophoblast transcript, *RYBP*, in COVID-19 groups, but this transcript was absent in Controls.
299 Both proteins encoded by these genes are involved in transcriptional regulation (*57, 58*). Several
300 of the unique mRNAs in EVs isolated from COVID-19 groups have been previously reported to
301 be associated with adverse pregnancy outcomes, including gestational hypertension,
302 preeclampsia, preterm birth, and intrauterine growth restriction (Supplemental Table 5). The
303 number of these pregnancy complication-associated mRNAs was highest in AI EVs, but they
304 were also abundant in EVs isolated from participants with resolved infections. Interestingly, the
305 abundance of eleven transcripts that have been implicated in preeclampsia differed between AI
306 EVs and Control EVs. Of importance, participants with AI also had a higher incidence of
307 preeclampsia. Moreover, two transcripts associated with preterm birth were uniquely carried in
308 R2, but not Control EVs; R2 participants had a higher incidence of preterm birth. This suggests
309 that EV cargo may reflect etiological pathways leading to these pregnancy complications.

310 **Circulating EVs carry transcriptional regulators of differentially expressed genes in the**
311 **placenta**

312 Because EVs had a direct functional effect on trophoblasts *in vitro*, we investigated
313 whether they carried transcriptional regulators of genes whose expression was altered in placenta
314 of COVID-19 pregnant participants (Supplemental Table 3). Multiple mRNAs encoding
315 transcriptional regulators were differentially abundant in COVID-19 groups compared to
316 Controls. Several were contained in both small and large EVs (*JUN, FOS, LEPR, LGALS1,*

317 *CD36*) or only in small EVs *(PRKN*). Moreover, Jun proto-oncogene B (*JUNB*) mRNA levels
318 were increased in large EVs from R1 compared to Controls (FC=2.25, p=0.01). This suggests
319 that *JUNB* carried in EVs could elicit the observed changes in transcription of its downstream
320 targets in the placenta. Similarly, mRNAs encoding 4 of the transcriptional regulators in R3
321 compared to Control placenta were found in large and small EVs (*IL1B, HIF1A, IGF2, PCBP1*);
322 1 was only in large EVs (*CXCR4*), and 3 were only in small EVs (*ESR1, AKT1, TP53, SPZ1,*
323 *IRS2*). Interestingly, interleukin 1 beta (*IL1B*) mRNA was decreased in large EVs from R3
324 compared to Controls (FC = -1.85, p=0.070), whereas estrogen receptor 1 (ESR1) mRNA levels
325 were lower in R3 small EVs compared to Controls (FC=-6.99, p=0.13). Importantly, expression
326 of genes controlled by these transcriptional regulators was altered in R3 placenta compared to
327 Controls. Similarly, many transcriptional regulators of genes with differential expression in AI
328 compared to Control placenta were found in both large and small EVs (*GRN* and *IL1B*), in large
329 EVs (*FAS*) or in small EVs (*JUN, STAT3, IFG1, IFNG, AGT*). These observations exemplify
330 potential EV-driven signaling leading to altered gene expression in the placenta that occurs in
331 COVID-19.

332 **DISCUSSION**

333 The long-term effects of COVID-19 during pregnancy have not yet been elucidated.
334 Previous studies and our findings reported here, show that the placenta is damaged, and the
335 likelihood of adverse pregnancy outcomes was increased in patients with a pregnancy
336 complicated by COVID-19. We have begun to elucidate the mechanisms underlying the
337 observed placental abnormalities associated with COVID-19. For the first time, we demonstrate
338 that circulating EVs from COVID-19 affected pregnancies 1) have a detrimental effect on
339 trophoblast function, including hormone production and invasion *in vitro*; 2) are altered after

340 SARS-CoV-2 infection; and 3) carry cargo that has been previously associated with adverse
341 pregnancy outcomes.

342 Our findings, in *in vitro* experiments, that trophoblast dysfunction following exposure to
343 EVs isolated from study participants with an active SARS-CoV-2 infection provides evidence
344 that circulating EVs contribute to the resulting placental pathology. We focused our *in vitro*
345 trophoblast experiments on the response to EVs isolated from participants with an active
346 infection because the magnitude of alteration in the placental transcriptome was greater
347 compared to those placentas from resolved infections. EVs from patients with an active
348 infection (AI) disrupted fundamental trophoblast functions that are crucial to maintain a healthy
349 pregnancy. Others have shown that trophoblast dysfunction, including failure to invade and
350 produce hormones, contributes to the development of preeclampsia, preterm birth, and
351 intrauterine growth restriction (*50, 51*). Therefore, the AI EV-induced reduction in EVT
352 invasion and syncytiotrophoblast hormone production may have contributed to the development
353 of these pregnancy complications following COVID-19.

354 Gestational age at the time of infection was a major determinant of COVID-19-induced
355 changes in the profile of circulating EVs. If participants were infected during the first or second
356 trimester of pregnancy, numbers of trophoblast and fetal endothelial cell large EV were
357 increased, and circulating large EVs carried more mtDNA. This suggests that COVID-19 during
358 early pregnancy disrupts mitochondrial function in the placenta. Mitochondrial dysfunction has
359 been reported in many organs following SARS-CoV-2 infection and is thought to contribute to
360 cell injury, cell death, and inflammation (*59-61*). Appelman et al. recently reported persistent
361 mitochondrial dysfunction in skeletal muscle long after the resolution of SARS-CoV-2 infection
362 (*62*). Further, elevated cell-free circulating mtDNA is commonly observed in COVID-19 and

363 correlates with severity and length of infection, reflecting significant mitochondria stress (*63-*
364 *66*). In support of a direct association of infection and mtDNA release in EVs, Faizan et al.
365 recently demonstrated that SARS-CoV-2 infection causes mitochondrial dysfunction and release
366 of EVs containing mtDNA in airway epithelial cells (*60*). Thus, our results suggest that
367 abnormal mitochondria may also play a role in the pathogenesis of placental dysfunction in
368 COVID-19.

369 Circulating EV cargo reflects the activity of the cells of origin. The transcripts carried by
370 EVs encode genes related to inflammation, vasculopathies, bioenergetics, and cell death,
371 processes and pathways that were present in the transcriptome and histopathology of the placenta
372 regardless of the timing of infection. EVs carry transcripts that are highly expressed by
373 trophoblasts, and have known functions in cellular metabolism, immune regulation, and
374 transcription. We also found that many of the transcripts in EVs from pregnancies complicated
375 by COVID-19 are encoded by genes that have been implicated in adverse pregnancy outcomes
376 including gestational hypertension, preeclampsia, preterm birth, and intrauterine growth
377 restriction. This points to shared pathways of placental dysfunction induced by a systemic
378 SARS-CoV-2 infection.

379 EV cargo can elicit a functional response when delivered to a recipient cell, as
380 demonstrated by our *in vitro* studies. While it is not known if mtDNA in EVs per se was
381 responsible for altering trophoblast function in our experiments, multiple studies have
382 demonstrated that mitochondria cargo can alter the recipient cell's mitochondrial function (*67-*
383 *69*). mRNA transcripts are also biologically active in recipient cells and we identified transcripts
384 in EVs that encode for multiple transcriptional regulators genes whose expression was altered in
385 placenta following COVID-19. Importantly, expression of several of these genes has been

386 previously reported to be altered in pregnancy complications. For example, JUN signaling was
387 disrupted in R1 placenta compared to Control placenta and JUNB mRNA was increased in
388 Control compared to R1 large EVs. JUN proteins are important for placentation, and a loss of
389 JUN signaling is implicated in preeclampsia (*70, 71*). Thus, low levels of JUNB in COVID-19
390 EVs may indicate placental dysfunction which in turn could contribute to the later development
391 of preeclampsia, which is observed at higher rates in pregnancies complicated by COVID-19
392 (*72*). In R3 compared to Controls, hormone receptor signaling was identified as a top canonical
393 pathway and differentially expressed genes were regulated by ESR1. *ESR1* mRNA was
394 abundant in small EVs isolated from Controls but not R3. ESR1 signaling is vital for placental
395 function and pregnancy maintenance because estrogen signaling is obligate for angiogenesis and
396 vasculature control (*73*). In fact, genetic variations in *ESR1* are associated with recurrent
397 pregnancy loss and preeclampsia, and both adverse pregnancy outcomes are increased in
398 maternal SARS-CoV-2 infection during pregnancy (*74, 75*). Thus, our findings suggest
399 placental dysfunction may in fact be a result of EV cargo delivery.

400 Our study is limited by the number of symptomatic patients with an active infection at the
401 time of delivery. Despite only 14% of pregnant participants experiencing COVID-19 related
402 symptoms, their placentas had significant pathology and an altered transcriptome. This was
403 associated with an increased incidence of preeclampsia and medically indicated preterm birth in
404 asymptomatic and symptomatic AI cases. It's worth noting that EVs obtained from
405 asymptomatic individuals have been found to exert significant impacts on trophoblast function
406 when tested in vitro. This discovery highlights the importance of exploring the potential
407 consequences of EV exposure in asymptomatic patients and may have important implications for
408 understanding the role of EVs in reproductive health.

409 Our study has provided significant insights into the profile and functional consequences
410 of circulating extracellular vesicles in mothers who were infected with SARS-CoV-2. This study
411 is the first to demonstrate the negative impact of maternal circulating vesicles on trophoblast
412 function in COVID-19. By comparing the placental transcriptome and EV cargo content, we
413 have identified shared pathways that are associated with pregnancy complications caused by
414 maternal COVID-19 and other pregnancy-related disorders that are not well understood.
415

416 **MATERIALS AND METHODS**

417 **Patient cohort**

418 The COMET study was conducted at the Hospital of the University of Pennsylvania (HUP) with
419 Institutional Review Board approval (IRB#843277). Study participants received a description of
420 the study and signed an informed consent before enrollment. Participants were enrolled at the
421 time of delivery in the COMET study between April 2020-June 2022. Participants were tested
422 for a SARS-CoV-2 infection by nasopharyngeal polymerase chain reaction (PCR) upon
423 admission to the labor and delivery unit at HUP. Participants who tested positive at the time of
424 delivery were enrolled in the active infection (AI) group. Those participants who tested negative
425 and had no known SARS-CoV-2 infection during their pregnancy were defined as Controls.
426 Participants with a negative test at delivery and a history of SARS-CoV-2 infection during their
427 pregnancy and greater than 14 days before enrollment, were defined as having a resolved
428 infection (R). All COVID-19 cases were unvaccinated against SARS-CoV-2. The gestational
429 age of SARS-CoV-2 infection was calculated, and participants were further divided into the
430 trimester of infection (resolved infection in the first trimester (R1), resolved infection in the
431 second trimester (R2) and resolved infection in the third trimester (R3)).

432 **Clinical and demographic data collection**

433 Clinical characteristics, such as maternal age, self-identified race, gestational age at
434 infection, and pregnancy outcomes, were extracted from the medical record (Table 1). The
435 severity of COVID-19 disease was categorized based on the National Institute of Health and
436 Society for Maternal-Fetal Medicine definitions: Asymptomatic infection was defined as
437 participants who tested positive but experienced no symptoms. Symptomatic participants
438 included all levels of illness (mild-critical).

439 **Sample collection**

440 Placentas were collected at the time of delivery. All placentas were examined by the
441 pathology department at the Hospital of the University of Pennsylvania (HUP). Placentas were
442 assessed using a systematic protocol that includes recording the trimmed placental weight,
443 membrane insertion site, gross appearance, dimensions of the placental disc, and umbilical cord
444 insertion, length, and diameter. Full-thickness placental biopsies were collected from an area
445 devoid of obvious pathology located equidistant between the placental cord insertion and the
446 edge of the placenta. Tissue was fixed in 10% formalin for histological assessment.
447 Macroscopic and microscopic lesions were identified and classified according to the Amsterdam
448 Placental Workshop Group 2014 classification (*76-78*). Placental biopsies were also collected
449 and stored in Trizol for RNA isolation.

450 Blood was collected at delivery in an EDTA tube and spun at 1,000G for 10 minutes at
451 room temperature to isolate plasma, which was aliquoted and stored at -80°C.

452 **Placenta and BeWo RNA isolation and sequencing**

453 Total RNA was isolated from placental biopsy samples using Qiagen RNEasy Plus Mini
454 Kits (Cat# 74134 Qiagen, Hilden, Germany). Total RNA was isolated from syncytialized BeWo
455 cells with the PicoPure RNA Isolation Kit (Cat# KIT0204 Applied Biosystems, Waltham, MA).
456 Isolated RNA was sent to NovoGene for library preparation and sequencing.

457 RNA integrity and quantification were assessed using the RNA Nano 6000 Assay Kit of
458 the Bioanalyzer 2100 System (Agilent Technologies, CA, USA). RNA purity was determined
459 using a NanoPhotometer spectrophotometer (IMPLEN, CA, USA). A total of 1μg RNA per
460 sample was used as input material for the RNA sample preparation. Sequencing libraries were
461 generated using NEBNext Ultra RNA Library Prep Kit for Illumina (NEB, USA) following
462 manufacturer recommendations, and index codes were added to identify samples. Clustering of
463 the index-coded samples was performed on an Illumina Novaseq 6000 sequencer according to
464 the manufacturer's instructions. After cluster generation, libraries were sequenced, and pair-end
465 reads were generated. Raw data (raw reads) of FASTQ format were processed through fastp. and
466 clean data was obtained by removing reads containing adapter and poly-N sequences and reads
467 with low quality. Pair-end clean reads were aligned to the GRCh38/hg38 reference genome
468 using Spliced Transcripts Alignment to a Reference (STAR) software. FeatureCounts were used
469 to count the read number mapped to each gene. Then RPKM of each gene was calculated based
470 on the length of the gene and read count mapped to the gene. Differential gene expression
471 between COVID-19 groups and Controls was assessed by DESeq2. Differentially expressed
472 genes were determined based on their adjusted p-value (<0.05) and >1.5-fold change. Functional
473 analysis was conducted using Qiagen's ingenuity pathway analysis (IPA). The clusterProfiler R
474 package was used to perform a Gene Ontology enrichment analysis of genes that were

475 differentially expressed. Canonical pathways, transcriptional regulators, and GO terms were
476 considered significant if the p-value was less than 0.05.

477 **EV isolation and characterization**

478 Serial centrifugation was utilized to isolate EVs from plasma. One mL of plasma was
479 spun in an Eppendorf 5424 benchtop centrifuge at 2,000 x g for 10 minutes at 4°C. The
480 supernatant was then spun at 20,000 x g for 30 minutes at 4°C. The pellet was washed in 1mL
481 filtered PBS and spun again at 20,000 x g for 30 minutes at 4°C. The large EV pellet was
482 resuspended in 100uL filtered PBS. The supernatant was spun by the Beckman Ultracentrifuge
483 Optima Max TL using the TLA 120.2 rotor at 100,000 x g (48,000RPM) for 90 minutes at 4°C.
484 The pellet was washed with 1mL filtered PBS and spun again at 100,000 x g (48,000RPM) for
485 90 minutes at 4°C. The small EV pellet was resuspended in 100uL filtered PBS.

486 EV isolation was confirmed by transmission electron microscopy, nanoparticle tracking,
487 and protein measurement as recommended by the MISEV guidelines (*79*). Transmission
488 electron microscopy images were generated and resulting images reviewed for the presence of
489 EVs. EVs were analyzed by Particle Metrix Zetaview nanoparticle tracking. 11 fields were
490 captured using the following parameters: sensitivity 80, frame rate 30, shutter 100, minimum
491 brightness 1000, minimum area 10, trace length 15. Representative histograms and TEM images
492 for large and small EVs are included in Supplemental Figure 1. CD9 protein abundance was
493 determined by gel electrophoresis. Total protein was measured with a Qubit Protein Assay Kit
494 and EV suspension was evaporated by vacuum and resuspended in electrophoresis buffer. Three
495 large EV (5µg) and small EV (20µg) samples were loaded into BioRad Mini-Protean TGX Gel
496 4-20% polyacrylamide gels with Licor Chameleon Duo ladders (928-60000) and run at 20mA

497 for 2 hours. Proteins were transferred to nitrocellulose membrane via 200mA over 3 hours on
498 ice. The membrane was blocked in Licor Intercept Blocking Buffer for 1hour at room
499 temperature then incubated with CD9 antibody (HI9a Biolegend Cat 312112) at 1:5000
500 overnight at room temperature. The membrane was then incubated with Licor IRDye 800CW
501 streptavidin (926-32230) at 1:5000 for 2 hours at room temperature and the membrane was
502 imaged by Licor Odyssey.

503 **Flow cytometry on EVs**

504 EVs surface protein expression was determined by flow cytometry following the MISEV
505 guidelines (*79*). EVs were resuspended at $1x10^8$/10μL of filtered PBS. Di-8-ANEPPS
506 (Invitrogen Cat# D3167) was reconstituted in ethanol as per manufacturer instruction and further
507 diluted to 1:1000 in filtered PBS. Antibodies were spun at 20,000 x g for 30 minutes at 4°C
508 immediately before use. 10μL of EV suspension was incubated in ANEPPS (10μL) and
509 antibodies, 1.25μL CD45-Ry586 (Cat# BD568135), 1.25μL CD41a- PE/Cy7 (Cat#
510 BDB561424), 1.25μL PLAP- eFlour660 (Fisher Cat# 50-112-4573) , and 1.25μL CD34-
511 PE/CF594 (Cat# BDB562449) and 3μL CD31-AF700 (Biolegend Cat# 50-207-2950), for 30
512 minutes at room temperature. 470μL of filtered PBS was added before samples were measured
513 by BD Symphony A1 cytometer which has improved sensitivity for small particles. Negative
514 controls included: antibodies alone, EVs without Di-8-ANEPPS, and EVs treated with 1% triton.
515 Data was analyzed using FlowJo software. EVs were identified by Small Particle Side Scatter
516 (SP-SSC) and expression of Di-8-ANEPPS and the relative proportion that expresses cell-
517 specific surface proteins was determined by antibody detection.

518 ***In vitro* trophoblast EV co-culture**

519 Extravillous trophoblasts (EVTs) were isolated from fresh first trimester placenta based
520 on an EVT outgrowth-based protocol established by Gram et al. (*80-84*). In brief, villous tissue
521 was finely minced and cultured at 37°C and 5% CO_2 in RPMI 1640 media with 20% FBS. After
522 attachment, EVT outgrowth occurs, and those cells were isolated. Isolated EVTs were confirmed
523 by staining for HLA-G and CK7. EVT invasion was measured using the MilliporeSigma
524 Chemicon QCM Collagen Cell Invasion Assay (Cat# ECM558). EVTs were added to the trans-
525 well invasion plate with EV-depleted media and large and small EVs at $1x10^6$/mL. Cells were
526 incubated at 37°C and 5% CO_2 for 48 hours. Cells that invaded through the collagen membrane
527 were quantified using a fluorescent plate reader (SpectraMax).

528 BeWo cells, subclone B30, were cultured in 75-cm^2 flasks (Fisher Scientific) at 37°C and
529 5% CO_2 in media (DMEM/F12, 10% FBS, 1% P/S, 1%L-alanyl-L-glutamine). EV-depleted
530 media was made with EV-depleted FBS (Gibco A2720801) and used for cell culture
531 experiments. Cells were plated at 250,000 cells/well in a 6 well plate and 1.5mL of EV-depleted
532 media was added. Cells adhered for 24 hours before adding 1μg/μL forskolin, a cAMP
533 producer, to promote syncytialization for an additional 24 hours. Large and small EVs were
534 resuspended in EV-depleted media at $1x10^6$/mL and added to BeWo cells for an additional 24
535 hours. At the time of harvest, cell media was collected, and cells released with 0.25% trypsin.
536 Cells were washed and collected as pellets for total DNA measurement and RNA isolation and
537 sequencing. Cell media was spun at 500 x g to clear cell debris and the supernatant was stored
538 for future hormone measurement. Hormones were measured by Penn Fertility Care using
539 Elecsys HCG+β (Cat# 03271749, Roche Diagnostics) and Elecsys Progesterone III (Cat#
540 07092539, Roche Diagnostics).

541 **EV mtDNA measurement**

542 mtDNA was isolated and quantified from large and small EVs by TaqMan-based
543 quantitative polymerase chain reaction (qPCR). We determined that $2x10^7$ large EV and $3x10^9$
544 small EVs were necessary to reliably and robustly measure mtDNA. As previously described,
545 we quantified mitochondrial-encoded human NADH: ubiquinone oxidoreductase core subunit 1
546 (ND1) as previously described (*85*). The qPCR reactions were performed in triplicates using a
547 QuantStudio 5 Real-time PCR System (Thermo Fisher) using the following thermocycling
548 conditions: 95 °C for 20 s followed by 40 cycles of 95 °C for 1 s, 63 °C for 20 s, and 60 °C for
549 20 s. Serial dilutions of pooled human placenta DNA quantified for copies of ND1 (copies/ μL)
550 by digital PCR (dPCR) were used as a standard curve. The mtDNA amount per EV was
551 determined by normalizing the resulting abundance by the number of EVs in starting material.
552 We calculated the Pearson correlation coefficient to determine the strength of the relationship
553 between gestational age at infection and abundance of EV mtDNA.

554 **EV mRNA sequencing**

555 Total RNA was isolated from large and small EVs isolated from 500μL of plasma.
556 Isolated EVs were treated with RNAseA (0.02μg/μL) (Invitrogen Cat# 12091021) for 20
557 minutes at 37°C to degrade extravesicular RNA. Enzyme activity was stopped by freezing
558 samples at -80°C for 5 minutes and immediate resuspension in Trizol. Nucleic acids were
559 isolated via BCP co-incubation, precipitated by isopropanol, and washed in ethanol. mRNA
560 libraries were prepared from total RNA using the SMART-Seq protocol (*86*). Briefly, RNA was
561 reverse transcribed using Superscript II (Invitrogen, Cat#18064014). The cDNA was amplified
562 with 20 cycles and cleaned up with AMPure XP beads (Beckman Coulter Cat#A63881). cDNA
563 was quantified with Qubit dsDNA HS Assay Kit (Life Technologies, Inc. Cat#Q32851), and 2ng
564 of each sample was used to construct a pool of uniquely indexed samples (Illumina Cat# FC-

565 131-1096). A second amplification was performed with 12 cycles and cleaned up with AMPure
566 XP beads. The final library was sequenced on a NextSeq 1000. Data were mapped against the
567 hg19 genome using RSEM and normalized to transcripts per million (tpm)(*87*).

568 To determine unique expression, we filtered genes to those that had greater than 5 tpm.
569 Unique genes had no expression (≤5 tpm) in all samples in the reference group and had
570 expression (>5 tpm) in the majority (≥ 50% of the samples) in the comparison group (data in
571 Table 2). Expression of unique genes in Controls, but not COVID-19 groups are shown in
572 Figure 4. These strict criteria identified genes in each group that were uniquely expressed, and
573 those genes were considered for subsequent analysis.

574 **Statistical analysis**

575 Statistical analysis was performed using GraphPad Prism. Differences in participant
576 demographics and outcomes were tested by a chi-squared test and considered statistically
577 different if $p<0.05$. Data was tested for normality and either parametric or non-parametric tests
578 were used to determine significance. Data points were identified as outliers and removed if they
579 exceeded two times the standard deviation from the mean. A one-way ANOVA tested for a
580 difference within all groups and subsequent post-hoc t-tests or Kruskal-Wallis determined the
581 significance of each COVID-19 group compared to Controls. Pearson's correlation was used to
582 determine a correlation between gestational age at infection and mtDNA abundance. A p-value
583 less than 0.05 was considered significant. Differential gene expression was determined to be
584 significant if the adjusted p-value was less than 0.05 and the fold change greater than 1.5.

585

586

587 **List of Supplementary Materials**

588 Supplemental Figure 1. EV Characterization

589 Supplemental Table 1. Placenta RNAseq DEG

590 Supplemental Table 2. Placenta RNAseq canonical pathways

591 Supplemental Table 3. Placental RNAseq transcriptional regulators

592 Supplemental Table 4. BeWo RNAseq pathway analysis

593 Supplemental Table 5. EV Transcripts Associated with Adverse Pregnancy Outcomes

594 References (*97-138*)

595

596 **References and Notes**

597 **Acknowledgments:** The authors would like to acknowledge the dedication and effort by the
598 Pregnancy and Perinatal Research Center, especially Meaghan McCabe, MPH, in
599 enrolling patients and collecting samples. The authors would also like to thank Dr. Luca
600 Musante at the University of Pennsylvania's Extracellular Vesicle Core for guidance in
601 EV-related methods. Finally, the authors would like to thank Dr. Jonni Moore and
602 Richard Schretzenmair at the University of Pennsylvania's Cytomics and Shared
603 Resource Laboratory for their guidance in conducting flow cytometry on EVs.

604 **Funding:**

605 Analyses of placentas collected at delivery (part of the COMET study) were supported (in part)
606 by a COVID-19 grant from the March of Dimes (SP, RAS)

607 National Institute of Health grant T32ES019851 (TNG)

National Institute of Health grant P30ES013508 (TNG)

Author contributions:

Experimental Design: TNG, SM, RLL, RL, LA, MM, CCC, BAK, JFS, SP, RAS

Data acquisition and analysis: TNG, SM, RLL, AW, LA, CCC, BAK

Writing- original draft: TNG, JFS, SP, RAS

Writing- review & editing: TNG, SM, RLL, RL, NAT, AW, LA, MM, CCC, BAK, JFS, SP, RAS

Competing interests: The authors declare they have no competing interests.

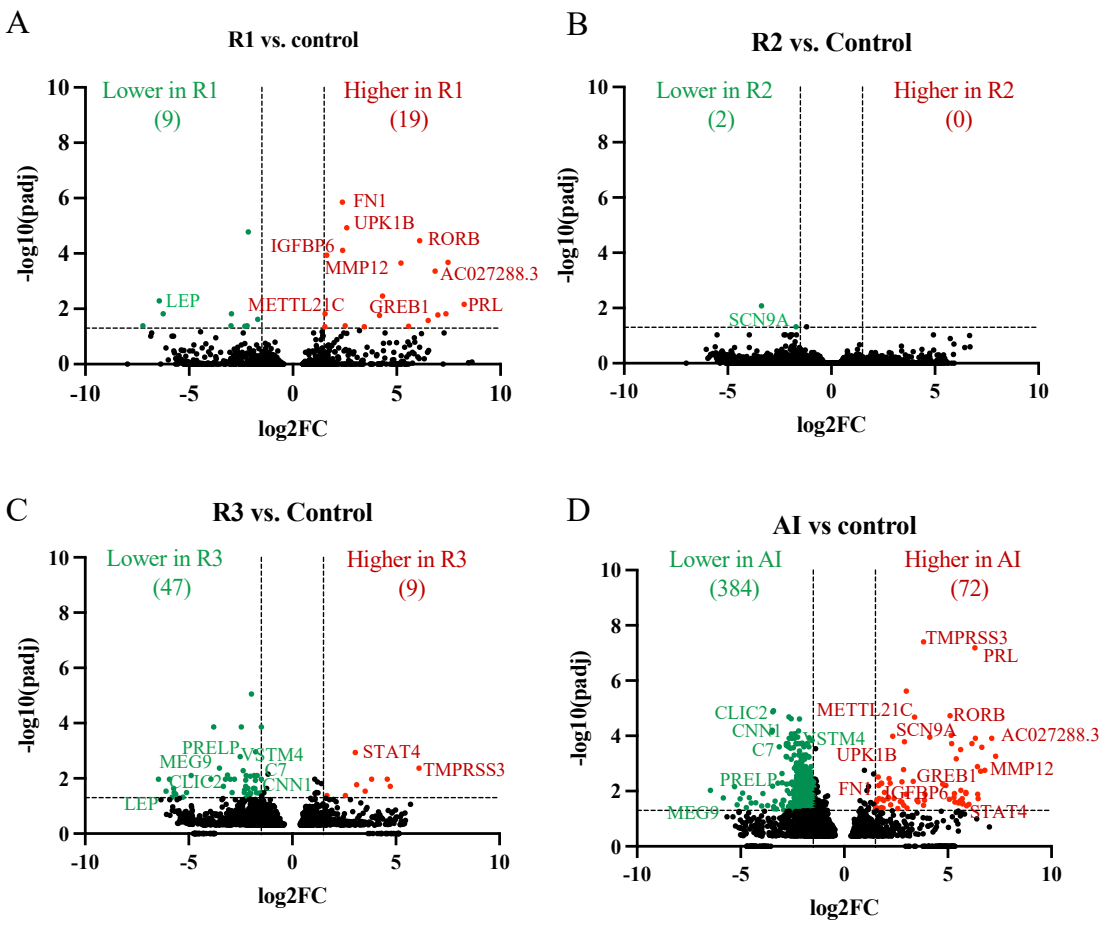

Figure 1. Differential gene expression in the placentas from patients with COVID-19 during pregnancy are represented by volcano plots. **(A-D)** The number and direction of differentially expressed genes between Controls (n=5) and resolved infections in the first trimester (R1) (A), second trimester (R2) (B), and third trimester (R3) (C), and active infection (AI) (D) is listed at the top of each graph. The gene name for those transcripts with differential expression in more than one COVID-19 group compared to Control is listed. (n=3-5/group)

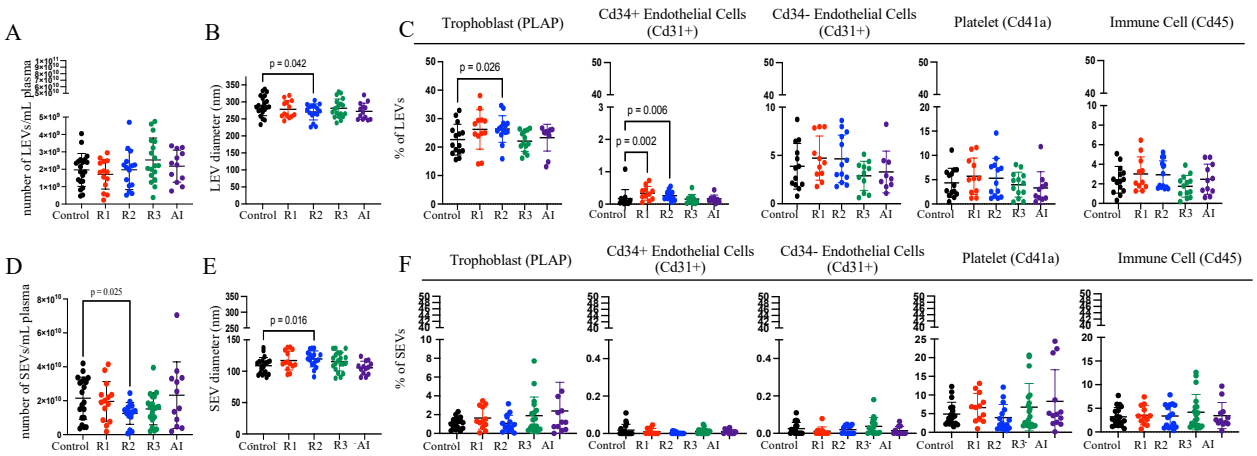

Figure 2. Circulating EVs were persistently altered in participants who experienced COVID-19 in the second trimester. **(A)** The number of LEVs in the circulation at the time of delivery (n=14-22/group). **(B)** The diameter of LEVs in the circulation (n=14-22/group). **(C)** Relative frequency of LEVs derived from trophoblasts, endothelial cells, platelets, and immune cells (n=11-16). **(D)** The number of small EVs in the circulation at the time of delivery (n=14-22/group). **(E)** The diameter of small EVs in the circulation (n=14-22/group). **(F)** The relative frequency of small EVs derived from endothelial cells, platelets, immune cells, and trophoblasts (n=13-20/group). All data are presented as mean ± SD. All analyses were performed by one-way ANOVA or the Kruskal-Wallis test, followed by post-hoc tests. Comparisons were made between Controls and resolved infection in the first trimester (R1), second trimester (R2), third trimester (R3), and active infection (AI).

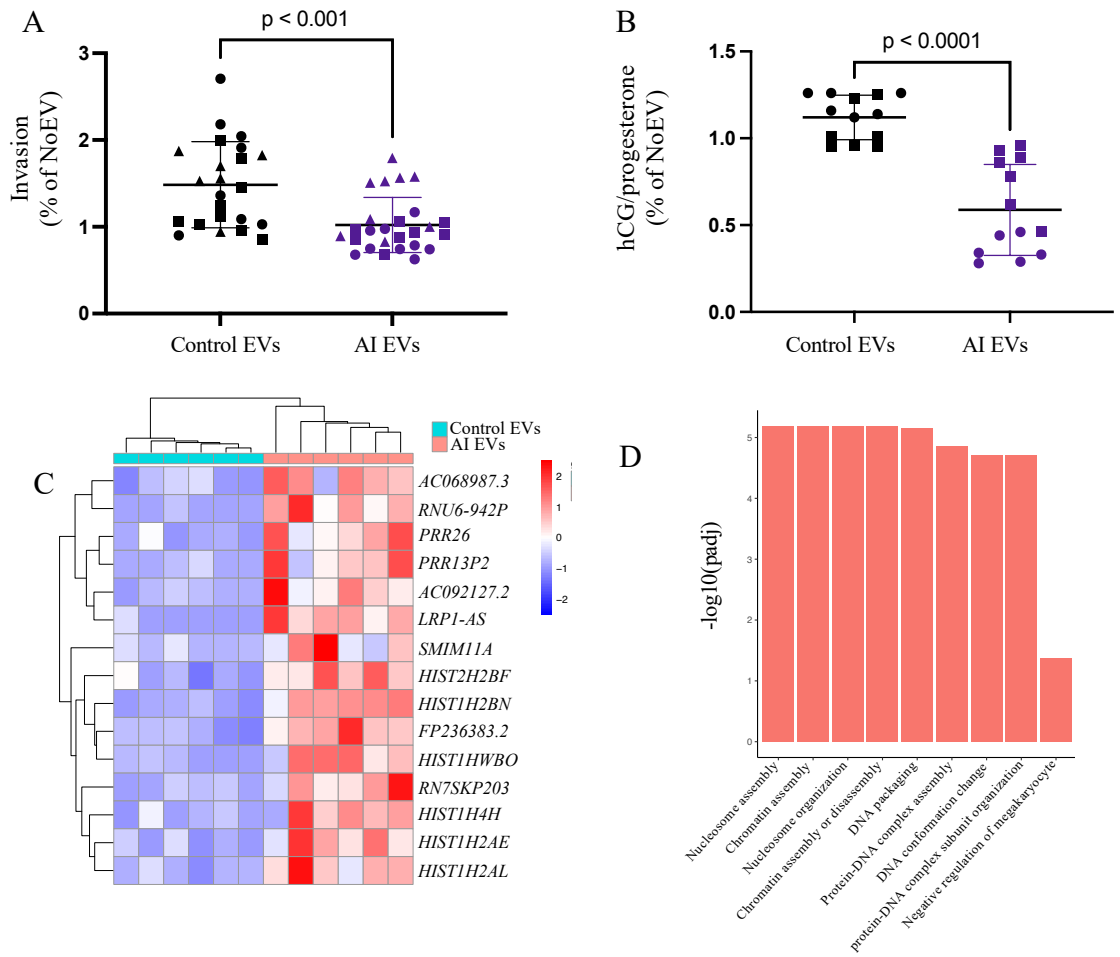

638

639 Figure 3. Trophoblast function was disrupted by exposure to EVs isolated from patients with an
640 active infection (AI) compared to Controls. **(A)** Extravillous trophoblasts (EVTs) were isolated
641 from three placentas (identified by symbol shape) and exposed to Control or AI EVs (n=9-
642 10/group, 3 experiments). Invasion was calculated and normalized to invasion of EVTs derived
643 from the same placenta not exposed to EVs (noEVs). All data are presented as mean ± SD. **(B)**
644 Human chorionic gonadotropin (hCG) and progesterone were measured in the media of
645 forskolin-treated (syncytialized) BeWo cells. The ratio of hCG to progesterone was normalized
646 to hormone production by cells not exposed to EVs (noEVs). The results of two experiments
647 (identified by symbol shape) are reported in B. (n=6-7/group, 2 experiments). All analyses were

648 performed by one-way ANOVA or Kruskal-Wallis test, followed by post-hoc tests. **(C)**
649 Following EV exposure, BeWo cell transcriptome was measured, and the top differentially
650 expressed genes comparing the cellular response to AI EVs to Control EVs are listed in the heat
651 map (red represents increased and blue represents decreased expression). **(D)** The biological
652 processes altered by AI EVs compared to Control EVs were determined by Gene Ontology
653 enrichment analysis.
654

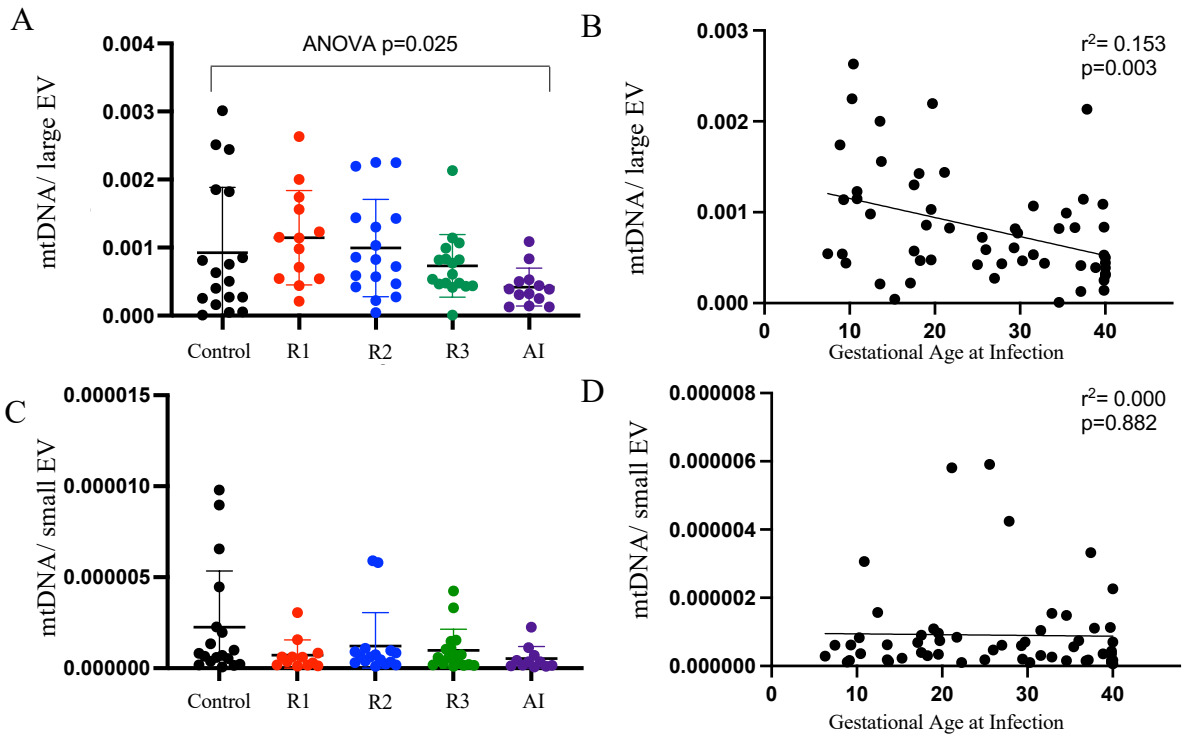

Figure 4. Large EV abundance of mtDNA is inversely correlated with gestational timing of infection. **(A&C)** The amount of mtDNA in each large EV (A) and small EV (C) is reported for each group (n=13-20/group). Data are presented as mean ± SD and tested by ANOVA followed by post-hoc tests. Independent pairwise comparisons were made between Controls and resolved infection in the 1st trimester (R1), second trimester (R2), third trimester (R3), or active infection (AI). **(B&D)** The Pearson correlation between gestational age at infection and mtDNA content is reported for large EV (B) and small EV (D).

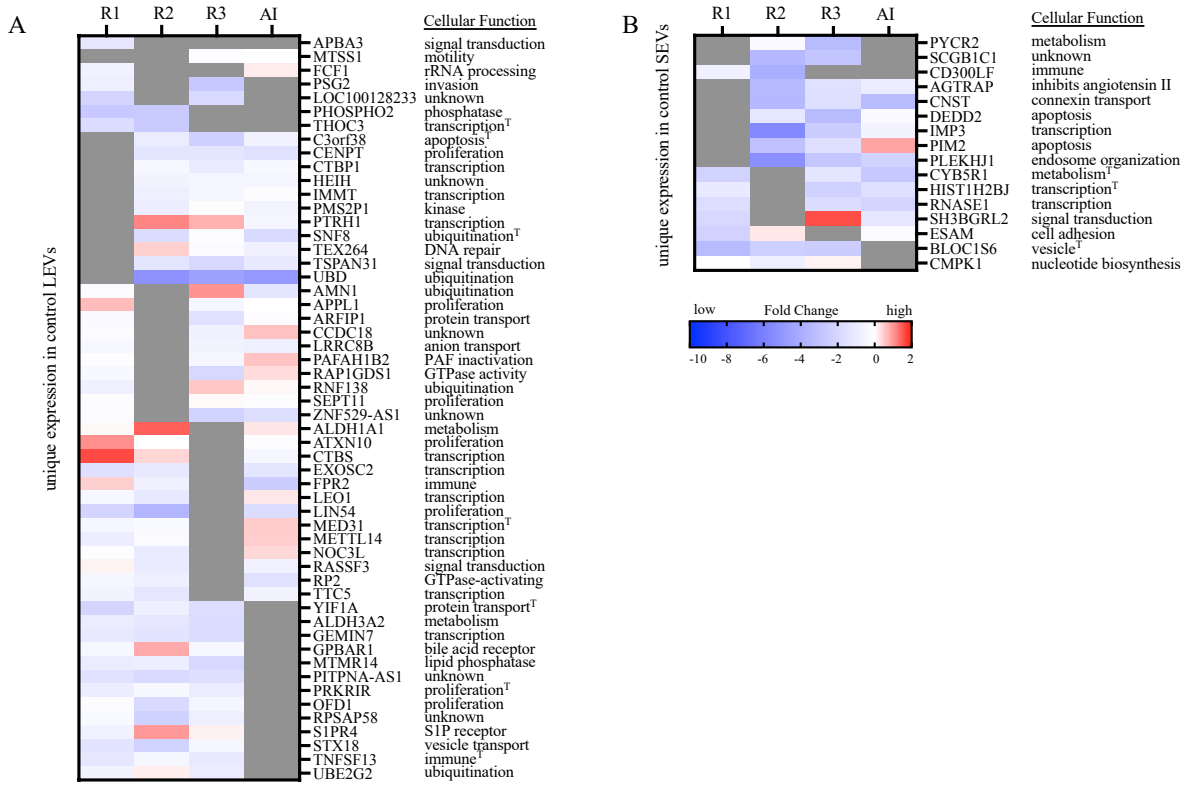

Figure 5. Control EVs carried transcripts that were absent in COVID-19 groups. **(A&B)** mRNA transcripts uniquely detected in EVs isolated from Controls but absent in EVs isolated from COVID-19 groups (gray bars) and differential expression (log 2-fold change) in other COVID-19 groups are listed in the heat map (increased expression is red and decreased expression is blue). The general cellular function of each gene product is listed on the right. Large EV transcripts are reported in (A) and small EV transcripts are reported in (B) (n=9-10/group). Independent pairwise comparisons were made between Controls and resolved infection in the first trimester (R1), second trimester (R2), third trimester (R3), or active infection (AI). Transcripts known to be highly abundant in trophoblasts are marked by (T).

Demographics	Controls (n=32)	R1 (n=15)	R2 (n=20)	R3 (n=22)	AI (n=21)
Maternal age (years)	21 – 42 (Mean: 31.8)	25 - 43 (Mean: 31.7)	18 – 39 (Mean: 29.4)	21 – 42 (Mean: 30.5)	20 – 40 (Mean: 29.4)
Race: White	50%	46.7%	34%	27.3%	9.5%*
Race: Black	41%	46.7%	55%	68.2%*	76.2%*
Race: Asian	9.4%	0%	10%	0%	9.5%
Race: Other/Unknown	0%	6.7%	0%	4.5%	4.8%
GA at delivery (weeks)	37.3 – 41.1 (Mean: 39.3)	35.1 – 40.3 (Mean: 39.1)	33.7 – 41.3 (Mean: 38.4)	32.3 – 39.7 (Mean: 37.5) *	31 – 41 (Mean: 38.1) *
COVID severity	Controls (n=32)	R1 (n=15)	R2 (n=20)	R3 (n=22)	AI (n=21)
Symptomatic	N/A	73.3%	85%	81.8%	14.3%
Asymptomatic	N/A	26.7%	15%	18.2%	85.7%$^{+}$
Hospitalized	N/A	13.3%	0%	31.8%	4.8%
Pregnancy outcomes	Controls (n=32)	R1 (n=15)	R2 (n=20)	R3 (n=22)	AI (n=21)
GHTN	18.8%	53.3%*$^{+}$	20%	13.6%	9.5%
CHTN	3.1%	0%	5%	13.6%	4.8%
Preeclampsia	0%	0%	5%	18.2%*	19%*
Spontaneous PTB	0%	0%	20%*	4.5%	4.8%
Medically indicated PTB	0%	6.7%	10%	18.2%*	19%*
IUGR	6.3%	13.3%	0%	9.1%	4.8%
IUFD	0%	0%	0%	4.5%	0%
Placenta Pathology	Control (n=26)	R1 (n=9)	R2 (n=17)	R3 (n=19)	AI (n=19)
MVM or FVM	26.9%	100%*	71%*	63%*	82.6%*
MVM	15%	44%*	47%*	37%	53%*
High grade MVM	0%	11%	18%*	16%*	11%
FVM	15%	78%*	59%*	42%*	47%*
>10% perivillous fibrin deposition	0%	11%	18%*	21%*	5%

Table 1. Subject demographics, pregnancy outcomes, and placenta pathology

Participants enrolled in the COMET study formed five groups (controls, resolved infection in the 1st trimester (R1), 2nd trimester (R2), and 3rd trimester (R3), and active infection (AI). Maternal demographics including maternal age, race, and gestational age (GA) at birth are reported. The severity of COVID-19 during their pregnancy, incidence of pregnancy complications (gestational hypertension (gHTN), chronic hypertension (cHTN), preeclampsia (PE), spontaneous and medically indicated preterm birth (PTB), intrauterine growth restriction (IUGR), and intrauterine demise (IUFD)) and placental pathology (maternal vascular malperfusion (MVM), fetal vascular malperfusion (FVM) and perivillous fibrin deposition) are reported * $p<0.05$ chi-squared test compared to Controls. $^{+}$ $p<0.05$ compared to other COVID-19 groups

685

Uniquely Expressed Transcripts in COVID EVs					
Gene Symbol	**Gene Name**	**Group(s) with Unique Expression**	**Cellular Function**	**High Trophoblast Expression**	**Increased in Pregnancy**
Large EVs					
YY1AP1	YY1 Associated Protein 1	R1, R2	Transcription		
MOSPD1	Motile Sperm Domain Containing 1	R1, AI	Transcription		
RYBP	RING1 And YY1 Binding Protein	R1, AI	Transcription	Y	
H1-4	H1.4 linker histone, cluster member	R2, R3	Unknown		
A2M	Alpha-2-Macroglobulin	R1	Immune		
KIFAP3	Kinesin Associated Protein 3	R1	Chromosome Movement		Y(*88*)
MXD1	MAX Dimerization Protein 1	R1	Proliferation		
PEX19	Peroxisomal Biogenesis Factor 19	R1	Oxidative stress	Y	
TOB1	Transducer Of ERBB2, 1	R1	Proliferation		
HK1	Hexokinase 1	R2	Metabolism	Y	
LY9	Lymphocyte Antigen 9	R2	Immune		Y(*89*)
POLR3C	RNA Polymerase III Subunit C	R2	Nucleic acid binding activity		
SPNS3	SPNS Lysolipid Transporter 3, Sphingosine-1-Phosphate (Putative)	R2	Transporter Activity		
WDR46	WD Repeat Domain 46	R2	Nucleic acid binding activity		
CDC34	Cell Division Cycle 34, Ubiquitin Conjugating Enzyme	R3	Ubiquitination		
FUNDC2	FUN14 Domain Containing 2	R3	Metabolism		
LINC-PINT	Long Intergenic Non-Protein Coding RNA, P53 Induced Transcript	R3	Unknown		
R3HCC1	R3H Domain and Coiled-Coil Containing 1	R3	Nucleic acid binding activity		
ATPSCKMT	ATP Synthase C Subunit Lysine N-Methyltransferase	AI	Mitochondrial ATP synthesis		
DTWD1	DTW Domain Containing 1	AI	Translation		
FBXL4	F-Box and Leucine Rich Repeat Protein 4	AI	Ubiquitination		
FRA10AC1	FRA10A Associated CGG Repeat 1	AI	Transcription		
FOXP1	Forkhead Box P1	AI	Transcription		
GOLGA4	Golgi A4	AI	Protein and lipid transport	Y	Y(*88*)

GPBP1L1	GC-Rich Promoter Binding Protein 1 Like 1	AI	Transcription		
IL1R2	Interleukin 1 Receptor Type 2	AI	Immune		
KIAA1143	KIAA1143	AI	Unknown		
LINC01410	Long Intergenic Non-Protein Coding RNA 1410	AI	Unknown		
NEAT1	Nuclear Paraspeckle Assembly Transcript 1	AI	Transcription	Y	
WDR26	WD Repeat Domain 26	AI	Cell cycle progression and gene regulation	Y	
XRN1	5'-3' Exoribonuclease 1	AI	mRNA degradation		Y(*90*)
ZNF638	Zinc Finger Protein 638	AI	Transcription		
Small EVs					
MYL4	Myosin Light Chain 4	R1, AI	Motor Protein		Y(*91*)
C18orf32	Chromosome 18 Open Reading Frame 32	R1, AI	Immune	Y	
CAPG	Capping Actin Protein, Gelsolin Like	R2, AI	Motor Protein		
CTSS	Cathepsin S	R3, AI	Immune		Y(*92*)
CYREN	Cell Cycle Regulator Of NHEJ	R1	DNA Repair		
CCDC124	Coiled-Coil Domain Containing 124	R1	Transcription		
CD27-AS1	CD27 Antisense RNA 1	R1	Immune		
GNB2	G Protein Subunit Beta 2	R1	G Protein Signaling		
PHF5A	PHD Finger Protein 5A	R1	Immune	Y	
RBM8A	RNA Binding Motif Protein 8A	R1	Transcription	Y	
SIGMAR1	Sigma Non-Opioid Intracellular Receptor 1	R1	Calcium Signaling	Y	
CSF3R	Colony Stimulating Factor 3 Receptor	R2	Immune	Y	
ESD	Esterase D	R2	Metabolism		
GTF2IRD2	GTF2I Repeat Domain Containing 2	R2	Transcription		
SLC1A5	Solute Carrier Family 1 Member 5	R2	Metabolism	Y	Y(*93*)
AUP1	AUP1 Lipid Droplet Regulating VLDL Assembly Factor	R3	Ubiquitination	Y	
MFF	Mitochondrial Fission Factor	R3	Mitochondrial and Peroxisomal Fission		
ARCN1	Archain 1	AI	Vesicle	Y	
CKAP2	Cytoskeleton Associated Protein 2	AI	Proliferation		Y(*94*)

CSNK2B	Casein Kinase 2 Beta	AI	Metabolism		
CYP27C1	Cytochrome P450 Family 27 Subfamily C Member 1	AI	Metabolism		
GRHL1	Grainyhead Like Transcription Factor 1	AI	Epithelial Development	Y	
HSP90B1	Heat Shock Protein 90 Beta Family Member 1	AI	Molecular Chaperone	Y	Y(*95*)
KIF5B	Kinesin Family Member 5B	AI	Protein Binding Activity		
LINC01123	Long Intergenic Non-Protein Coding RNA 1123	AI	Unknown		
LOC728323	Unknown	AI	Unknown		
MANBAL	Mannosidase Beta Like	AI	Membrane Protein		Y(*96*)
MUC22	Mucin 22	AI	Membrane Protein		
MYLK	Myosin Light Chain Kinase	AI	Contractile Activity		
OR4F17	Olfactory Receptor Family 4 Subfamily F Member 17	AI	Vesicle		
PARP9	Poly (ADP-Ribose) Polymerase Family Member 9	AI	Immune		
RNF2	Ring Finger Protein 2	AI	Transcription		
SAR1A	Secretion Associated Ras Related GTPase 1A	AI	Vesicle	Y	
SHC4	SHC Adaptor Protein 4	AI	Proliferation		
SRSF8	Serine And Arginine Rich Splicing Factor 8	AI	Transcription	Y	
TMCC2	Transmembrane And Coiled-Coil Domain Family 2	AI	Metabolism	Y	
TRIM4	Tripartite Motif Containing 4	AI	Immune		
TWF2	Twinfilin Actin Binding Protein 2	AI	Actin and ATP Binding Site		
VTA1	Vesicle Trafficking 1	AI	Vesicle		
ZNF484	Zinc Finger Protein 484	AI	Transcription		

686 Table 2. Unique genes identified in EVs isolated from COVID-19 cases

687 Transcripts are carried by large EVs or small EVs isolated from COVID-19 cases that are absent in

688 Controls. The listed transcripts are not detected in EVs isolated from Controls but are present in the

689 identified COVID-19 group(s). The cellular function, expression in trophoblasts, and pregnancy

690 associated expression of each transcript is listed as well (reference listed).

691 References:

692 1. A. Conde-Agudelo, R. Romero, SARS-CoV-2 infection during pregnancy and risk of preeclampsia: a
693 systematic review and meta-analysis. *Am J Obstet Gynecol* **226**, 68-89 e63 (2022).

694 2. E. R. Smith *et al.*, Adverse maternal, fetal, and newborn outcomes among pregnant women with SARS-
695 CoV-2 infection: an individual participant data meta-analysis. *BMJ Glob Health* **8**, (2023).

696 3. C. M. Corbetta-Rastelli *et al.*, Analysis of placental pathology after COVID-19 by timing and severity of
697 infection. *Am J Obstet Gynecol MFM* **5**, 100981 (2023).

698 4. F. M. Cribiu *et al.*, Severe SARS-CoV-2 placenta infection can impact neonatal outcome in the absence of
699 vertical transmission. *J Clin Invest* **131**, (2021).

700 5. B. Joshi *et al.*, The placental pathology in Coronavirus disease 2019 infected mothers and its impact on
701 pregnancy outcome. *Placenta* **127**, 1-7 (2022).

702 6. E. T. Patberg *et al.*, Coronavirus disease 2019 infection and placental histopathology in women delivering
703 at term. *Am J Obstet Gynecol* **224**, 382 e381-382 e318 (2021).

704 7. A. G. Edlow *et al.*, Assessment of Maternal and Neonatal SARS-CoV-2 Viral Load, Transplacental
705 Antibody Transfer, and Placental Pathology in Pregnancies During the COVID-19 Pandemic. *JAMA Netw*
706 *Open* **3**, e2030455 (2020).

707 8. J. J. Mulvey, C. M. Magro, L. X. Ma, G. J. Nuovo, R. N. Baergen, Analysis of complement deposition and
708 viral RNA in placentas of COVID-19 patients. *Ann Diagn Pathol* **46**, 151530 (2020).

709 9. C. Balbi *et al.*, Circulating extracellular vesicles are endowed with enhanced procoagulant activity in
710 SARS-CoV-2 infection. *EBioMedicine* **67**, 103369 (2021).

711 10. D. Forte *et al.*, Circulating extracellular particles from severe COVID-19 patients show altered profiling
712 and innate lymphoid cell-modulating ability. *Front Immunol* **14**, 1085610 (2023).

713 11. M. S. George *et al.*, Extracellular vesicles in COVID-19 convalescence can regulate T cell metabolism and
714 function. *iScience* **26**, 107280 (2023).

715 12. A. Rosell *et al.*, Patients With COVID-19 Have Elevated Levels of Circulating Extracellular Vesicle Tissue
716 Factor Activity That Is Associated With Severity and Mortality-Brief Report. *Arterioscler Thromb Vasc*
717 *Biol* **41**, 878-882 (2021).

718 13. L. Traby *et al.*, Extracellular Vesicles and Citrullinated Histone H3 in Coronavirus Disease 2019 Patients.
719 *Thromb Haemost* **122**, 113-122 (2022).
720 14. E. Barberis *et al.*, Circulating Exosomes Are Strongly Involved in SARS-CoV-2 Infection. *Front Mol*
721 *Biosci* **8**, 632290 (2021).
722 15. Y. Fujita *et al.*, Early prediction of COVID-19 severity using extracellular vesicle COPB2. *J Extracell*
723 *Vesicles* **10**, e12092 (2021).
724 16. K. Mao *et al.*, Proteomics of extracellular vesicles in plasma reveals the characteristics and residual traces
725 of COVID-19 patients without underlying diseases after 3 months of recovery. *Cell Death Dis* **12**, 541
726 (2021).
727 17. F. Puhm, L. Flamand, E. Boilard, Platelet extracellular vesicles in COVID-19: Potential markers and
728 makers. *J Leukoc Biol* **111**, 63-74 (2022).
729 18. K. H. W. Yim, S. Borgoni, R. Chahwan, Serum extracellular vesicles profiling is associated with COVID-
730 19 progression and immune responses. *J Extracell Biol* **1**, e37 (2022).
731 19. C. Salomon *et al.*, A gestational profile of placental exosomes in maternal plasma and their effects on
732 endothelial cell migration. *PLoS One* **9**, e98667 (2014).
733 20. S. Sarker *et al.*, Placenta-derived exosomes continuously increase in maternal circulation over the first
734 trimester of pregnancy. *J Transl Med* **12**, 204 (2014).
735 21. J. Ratajczak *et al.*, Paracrine proangiopoietic effects of human umbilical cord blood-derived purified
736 CD133+ cells--implications for stem cell therapies in regenerative medicine. *Stem Cells Dev* **22**, 422-430
737 (2013).
738 22. K. Bai *et al.*, Placenta-Derived Exosomes as a Modulator in Maternal Immune Tolerance During
739 Pregnancy. *Front Immunol* **12**, 671093 (2021).
740 23. X. Chang *et al.*, Exosomes From Women With Preeclampsia Induced Vascular Dysfunction by Delivering
741 sFlt (Soluble Fms-Like Tyrosine Kinase)-1 and sEng (Soluble Endoglin) to Endothelial Cells. *Hypertension*
742 **72**, 1381-1390 (2018).
743 24. I. Hromadnikova, L. Dvorakova, K. Kotlabova, L. Krofta, The Prediction of Gestational Hypertension,
744 Preeclampsia and Fetal Growth Restriction via the First Trimester Screening of Plasma Exosomal C19MC
745 microRNAs. *Int J Mol Sci* **20**, (2019).

746 25. P. Pillay, N. Maharaj, J. Moodley, I. Mackraj, Placental exosomes and pre-eclampsia: Maternal circulating
747 levels in normal pregnancies and, early and late onset pre-eclamptic pregnancies. *Placenta* **46**, 18-25
748 (2016).
749 26. C. Salomon *et al.*, Gestational Diabetes Mellitus Is Associated With Changes in the Concentration and
750 Bioactivity of Placenta-Derived Exosomes in Maternal Circulation Across Gestation. *Diabetes* **65**, 598-609
751 (2016).
752 27. M. Wilkinson, E. D. Johnstone, L. E. Simcox, J. E. Myers, The impact of COVID-19 on pregnancy
753 outcomes in a diverse cohort in England. *Sci Rep* **12**, 942 (2022).
754 28. N. Alcover *et al.*, Systematic review and synthesis of stillbirths and late miscarriages following SARS-
755 CoV-2 infections. *Am J Obstet Gynecol* **229**, 118-128 (2023).
756 29. K. Narang *et al.*, Impact of asymptomatic and mild COVID-19 infection on fetal growth during pregnancy.
757 *Eur J Obstet Gynecol Reprod Biol* **281**, 63-67 (2023).
758 30. R. N. Baergen, D. S. Heller, J. A. Goldstein, Placental Pathology in COVID-19. *Am J Clin Pathol* **154**, 279
759 (2020).
760 31. M. C. Sharps *et al.*, A structured review of placental morphology and histopathological lesions associated
761 with SARS-CoV-2 infection. *Placenta* **101**, 13-29 (2020).
762 32. T. Ohmaru-Nakanishi *et al.*, Fibrosis in Preeclamptic Placentas Is Associated with Stromal Fibroblasts
763 Activated by the Transforming Growth Factor-beta1 Signaling Pathway. *Am J Pathol* **188**, 683-695 (2018).
764 33. H. Li *et al.*, Human Placental Endothelial Cell and Trophoblast Heterogeneity and Differentiation Revealed
765 by Single-Cell RNA Sequencing. *Cells* **12**, (2022).
766 34. A. G. Foote, Z. Wang, C. Kendziorski, S. L. Thibeault, Tissue specific human fibroblast differential
767 expression based on RNAsequencing analysis. *BMC Genomics* **20**, 308 (2019).
768 35. F. Fang, Y. Yao, Z. Ma, Exploration of the Long Noncoding RNAs Involved in the Crosstalk between M2
769 Macrophages and Tumor Metabolism in Lung Cancer. *Genet Res (Camb)* **2023**, 4512820 (2023).
770 36. A. Liso *et al.*, IGFBP-6: At the Crossroads of Immunity, Tissue Repair and Fibrosis. *Int J Mol Sci* **23**,
771 (2022).
772 37. D. Chakraborty *et al.*, HIF-KDM3A-MMP12 regulatory circuit ensures trophoblast plasticity and placental
773 adaptations to hypoxia. *Proc Natl Acad Sci U S A* **113**, E7212-E7221 (2016).

774 38. H. Mogami *et al.*, Fetal fibronectin signaling induces matrix metalloproteases and cyclooxygenase-2
775 (COX-2) in amnion cells and preterm birth in mice. *J Biol Chem* **288**, 1953-1966 (2013).
776 39. Y. Okamura *et al.*, The extra domain A of fibronectin activates Toll-like receptor 4. *J Biol Chem* **276**,
777 10229-10233 (2001).
778 40. A. J. Camden *et al.*, Growth regulation by estrogen in breast cancer 1 (GREB1) is a novel progesterone-
779 responsive gene required for human endometrial stromal decidualization. *Mol Hum Reprod* **23**, 646-653
780 (2017).
781 41. S. B. Chadchan *et al.*, A GREB1-steroid receptor feedforward mechanism governs differential GREB1
782 action in endometrial function and endometriosis. *Nat Commun* **15**, 1947 (2024).
783 42. S. Biswas Shivhare, J. N. Bulmer, B. A. Innes, D. K. Hapangama, G. E. Lash, Altered vascular smooth
784 muscle cell differentiation in the endometrial vasculature in menorrhagia. *Hum Reprod* **29**, 1884-1894
785 (2014).
786 43. G. S. Whitley, J. E. Cartwright, Cellular and molecular regulation of spiral artery remodelling: lessons from
787 the cardiovascular field. *Placenta* **31**, 465-474 (2010).
788 44. B. Afzali, M. Noris, B. N. Lambrecht, C. Kemper, The state of complement in COVID-19. *Nat Rev*
789 *Immunol* **22**, 77-84 (2022).
790 45. C. B. Chighizola, P. A. Lonati, L. Trespidi, P. L. Meroni, F. Tedesco, The Complement System in the
791 Pathophysiology of Pregnancy and in Systemic Autoimmune Rheumatic Diseases During Pregnancy. *Front*
792 *Immunol* **11**, 2084 (2020).
793 46. L. Li *et al.*, Research progress on the STAT signaling pathway in pregnancy and pregnancy-associated
794 disorders. *Front Immunol* **14**, 1331964 (2023).
795 47. L. Zhang *et al.*, The diagnosis values of serum STAT4 and sEng in preeclampsia. *J Clin Lab Anal* **34**,
796 e23073 (2020).
797 48. O. Parant *et al.*, CD34+ cells in maternal placental blood are mainly fetal in origin and express endothelial
798 markers. *Lab Invest* **89**, 915-923 (2009).
799 49. C. Salomon *et al.*, Hypoxia-induced changes in the bioactivity of cytotrophoblast-derived exosomes. *PLoS*
800 *One* **8**, e79636 (2013).

801 50. P. Kaufmann, S. Black, B. Huppertz, Endovascular trophoblast invasion: implications for the pathogenesis
802 of intrauterine growth retardation and preeclampsia. *Biol Reprod* **69**, 1-7 (2003).
803 51. P. Tantbirojn, C. P. Crum, M. M. Parast, Pathophysiology of placenta creta: the role of decidua and
804 extravillous trophoblast. *Placenta* **29**, 639-645 (2008).
805 52. M. Prieto-Vila, Y. Yoshioka, T. Ochiya, Biological Functions Driven by mRNAs Carried by Extracellular
806 Vesicles in Cancer. *Front Cell Dev Biol* **9**, 620498 (2021).
807 53. M. C. Deregibus *et al.*, Endothelial progenitor cell derived microvesicles activate an angiogenic program in
808 endothelial cells by a horizontal transfer of mRNA. *Blood* **110**, 2440-2448 (2007).
809 54. J. Ratajczak *et al.*, Embryonic stem cell-derived microvesicles reprogram hematopoietic progenitors:
810 evidence for horizontal transfer of mRNA and protein delivery. *Leukemia* **20**, 847-856 (2006).
811 55. H. Valadi *et al.*, Exosome-mediated transfer of mRNAs and microRNAs is a novel mechanism of genetic
812 exchange between cells. *Nat Cell Biol* **9**, 654-659 (2007).
813 56. Z. Wei *et al.*, Coding and noncoding landscape of extracellular RNA released by human glioma stem cells.
814 *Nat Commun* **8**, 1145 (2017).
815 57. C. Shu, P. Xu, J. Han, S. Han, J. He, Upregulation of circRNA hsa_circ_0008726 in Pre-eclampsia Inhibits
816 Trophoblast Migration, Invasion, and EMT by Regulating miR-345-3p/RYBP Axis. *Reprod Sci* **29**, 2829-
817 2841 (2022).
818 58. L. Wang *et al.*, The THO complex regulates pluripotency gene mRNA export and controls embryonic stem
819 cell self-renewal and somatic cell reprogramming. *Cell Stem Cell* **13**, 676-690 (2013).
820 59. J. D. Domizio *et al.*, The cGAS-STING pathway drives type I IFN immunopathology in COVID-19.
821 *Nature* **603**, 145-151 (2022).
822 60. M. I. Faizan *et al.*, NSP4 and ORF9b of SARS-CoV-2 Induce Pro-Inflammatory Mitochondrial DNA
823 Release in Inner Membrane-Derived Vesicles. *Cells* **11**, (2022).
824 61. L. Gibellini *et al.*, Altered bioenergetics and mitochondrial dysfunction of monocytes in patients with
825 COVID-19 pneumonia. *EMBO Mol Med* **12**, e13001 (2020).
826 62. B. Appelman *et al.*, Muscle abnormalities worsen after post-exertional malaise in long COVID. *Nat*
827 *Commun* **15**, 17 (2024).

828 63. D. Scozzi *et al.*, Circulating mitochondrial DNA is an early indicator of severe illness and mortality from
829 COVID-19. *JCI Insight* **6**, (2021).
830 64. S. Shoraka, S. R. Mohebbi, S. M. Hosseini, M. R. Zali, Comparison of plasma mitochondrial DNA copy
831 number in asymptomatic and symptomatic COVID-19 patients. *Front Microbiol* **14**, 1256042 (2023).
832 65. J. J. Valdes-Aguayo *et al.*, Peripheral Blood Mitochondrial DNA Levels Were Modulated by SARS-CoV-2
833 Infection Severity and Its Lessening Was Associated With Mortality Among Hospitalized Patients With
834 COVID-19. *Front Cell Infect Microbiol* **11**, 754708 (2021).
835 66. T. J. Costa *et al.*, Mitochondrial DNA and TLR9 activation contribute to SARS-CoV-2-induced endothelial
836 cell damage. *Vascul Pharmacol* **142**, 106946 (2022).
837 67. L. Peruzzotti-Jametti *et al.*, Neural stem cells traffic functional mitochondria via extracellular vesicles.
838 *PLoS Biol* **19**, e3001166 (2021).
839 68. D. G. Phinney *et al.*, Mesenchymal stem cells use extracellular vesicles to outsource mitophagy and shuttle
840 microRNAs. *Nat Commun* **6**, 8472 (2015).
841 69. P. Sansone *et al.*, Packaging and transfer of mitochondrial DNA via exosomes regulate escape from
842 dormancy in hormonal therapy-resistant breast cancer. *Proc Natl Acad Sci U S A* **114**, E9066-E9075
843 (2017).
844 70. M. Schorpp-Kistner, Z. Q. Wang, P. Angel, E. F. Wagner, JunB is essential for mammalian placentation.
845 *EMBO J* **18**, 934-948 (1999).
846 71. A. M. Nuzzo *et al.*, JunB/cyclin-D1 imbalance in placental mesenchymal stromal cells derived from
847 preeclamptic pregnancies with fetal-placental compromise. *Placenta* **35**, 483-490 (2014).
848 72. A. T. Papageorghiou *et al.*, Preeclampsia and COVID-19: results from the INTERCOVID prospective
849 longitudinal study. *Am J Obstet Gynecol* **225**, 289 e281-289 e217 (2021).
850 73. N. Berkane *et al.*, From Pregnancy to Preeclampsia: A Key Role for Estrogens. *Endocr Rev* **38**, 123-144
851 (2017).
852 74. W. Bahia *et al.*, Association of genetic variants in Estrogen receptor (ESR)1 and ESR2 with susceptibility
853 to recurrent pregnancy loss in Tunisian women: A case control study. *Gene* **736**, 144406 (2020).
854 75. H. A. El-Beshbishy *et al.*, Estrogen Receptor Alpha (ESR1) Gene Polymorphisms in Pre-eclamptic Saudi
855 Patients. *Pak J Med Sci* **31**, 880-885 (2015).

856 76. A. A. Freedman, L. S. Keenan-Devlin, A. Borders, G. E. Miller, L. M. Ernst, Formulating a Meaningful
857 and Comprehensive Placental Phenotypic Classification. *Pediatr Dev Pathol* **24**, 337-350 (2021).
858 77. T. Y. Khong *et al.*, Sampling and Definitions of Placental Lesions: Amsterdam Placental Workshop Group
859 Consensus Statement. *Arch Pathol Lab Med* **140**, 698-713 (2016).
860 78. R. W. Redline, S. Ravishankar, C. M. Bagby, S. T. Saab, S. Zarei, Four major patterns of placental injury: a
861 stepwise guide for understanding and implementing the 2016 Amsterdam consensus. *Mod Pathol* **34**, 1074-
862 1092 (2021).
863 79. C. Thery *et al.*, Minimal information for studies of extracellular vesicles 2018 (MISEV2018): a position
864 statement of the International Society for Extracellular Vesicles and update of the MISEV2014 guidelines.
865 *J Extracell Vesicles* **7**, 1535750 (2018).
866 80. L. Anton, A. G. Brown, S. Parry, M. A. Elovitz, Lipopolysaccharide induces cytokine production and
867 decreases extravillous trophoblast invasion through a mitogen-activated protein kinase-mediated pathway:
868 possible mechanisms of first trimester placental dysfunction. *Hum Reprod* **27**, 61-72 (2012).
869 81. L. Anton *et al.*, HIF-1alpha Stabilization Increases miR-210 Eliciting First Trimester Extravillous
870 Trophoblast Mitochondrial Dysfunction. *Front Physiol* **10**, 699 (2019).
871 82. S. Getsios, G. T. Chen, D. T. Huang, C. D. MacCalman, Regulated expression of cadherin-11 in human
872 extravillous cytotrophoblasts undergoing aggregation and fusion in response to transforming growth factor
873 beta 1. *J Reprod Fertil* **114**, 357-363 (1998).
874 83. C. H. Graham, J. J. Lysiak, K. R. McCrae, P. K. Lala, Localization of transforming growth factor-beta at
875 the human fetal-maternal interface: role in trophoblast growth and differentiation. *Biol Reprod* **46**, 561-572
876 (1992).
877 84. J. Y. Park *et al.*, A microphysiological model of human trophoblast invasion during implantation. *Nat*
878 *Commun* **13**, 1252 (2022).
879 85. S. A. Ware *et al.*, An automated, high-throughput methodology optimized for quantitative cell-free
880 mitochondrial and nuclear DNA isolation from plasma. *J Biol Chem* **295**, 15677-15691 (2020).
881 86. J. J. Trombetta *et al.*, Preparation of Single-Cell RNA-Seq Libraries for Next Generation Sequencing. *Curr*
882 *Protoc Mol Biol* **107**, 4 22 21-24 22 17 (2014).

883 87. O. Yukselen, O. Turkyilmaz, A. R. Ozturk, M. Garber, A. Kucukural, DolphinNext: a distributed data
884 processing platform for high throughput genomics. *BMC Genomics* **21**, 310 (2020).
885 88. K. S. Rehman, S. Yin, B. A. Mayhew, R. A. Word, W. E. Rainey, Human myometrial adaptation to
886 pregnancy: cDNA microarray gene expression profiling of myometrium from non-pregnant and pregnant
887 women. *Mol Hum Reprod* **9**, 681-700 (2003).
888 89. C. M. Whittington *et al.*, Transcriptomic changes in the pre-implantation uterus highlight histotrophic
889 nutrition of the developing marsupial embryo. *Sci Rep* **8**, 2412 (2018).
890 90. S. Peng *et al.*, Genetic regulation of the placental transcriptome underlies birth weight and risk of childhood
891 obesity. *PLoS Genet* **14**, e1007799 (2018).
892 91. J. L. Maron *et al.*, Gene expression analysis in pregnant women and their infants identifies unique fetal
893 biomarkers that circulate in maternal blood. *J Clin Invest* **117**, 3007-3019 (2007).
894 92. G. Song, F. W. Bazer, T. E. Spencer, Differential expression of cathepsins and cystatin C in ovine
895 uteroplacental tissues. *Placenta* **28**, 1091-1098 (2007).
896 93. C. P. Chen *et al.*, Altered placental syncytin and its receptor ASCT2 expression in placental development
897 and pre-eclampsia. *BJOG* **113**, 152-158 (2006).
898 94. K. L. Fulghum *et al.*, Metabolic signatures of pregnancy-induced cardiac growth. *Am J Physiol Heart Circ*
899 *Physiol* **323**, H146-H164 (2022).
900 95. M. Prater *et al.*, RNA-Seq reveals changes in human placental metabolism, transport and endocrinology
901 across the first-second trimester transition. *Biol Open* **10**, (2021).
902 96. M. B. Rabaglino, J. M. Sanchez, M. McDonald, E. O'Callaghan, P. Lonergan, Maternal blood
903 transcriptome as a sensor of foetal organ maturation at the end of organogenesis in cattle. *Biol Reprod*,
904 (2023).
905 97. C. Y. Hung *et al.*, A defect in the inner kinetochore protein CENPT causes a new syndrome of severe
906 growth failure. *PLoS One* **12**, e0189324 (2017).
907 98. W. Li *et al.*, Role of IGF2BP3 in trophoblast cell invasion and migration. *Cell Death Dis* **5**, e1025 (2014).
908 99. H. Wen, L. Chen, J. He, J. Lin, MicroRNA expression profiles and networks in placentas complicated with
909 selective intrauterine growth restriction. *Mol Med Rep* **16**, 6650-6673 (2017).

910 100. G. Wang *et al.*, Impact of intrauterine exposure to maternal diabetes on preterm birth: fetal DNA
911 methylation alteration is an important mediator. *Clin Epigenetics* **15**, 59 (2023).
912 101. I. L. Aye, T. L. Powell, T. Jansson, Review: Adiponectin--the missing link between maternal adiposity,
913 placental transport and fetal growth? *Placenta* **34 Suppl**, S40-45 (2013).
914 102. I. Hromadnikova *et al.*, Expression profile of C19MC microRNAs in placental tissue in pregnancy-related
915 complications. *DNA Cell Biol* **34**, 437-457 (2015).
916 103. Y. Gu, S. A. Burlison, Y. Wang, PAF levels and PAF-AH activities in placentas from normal and
917 preeclamptic pregnancies. *Placenta* **27**, 744-749 (2006).
918 104. T. Garrido-Gomez *et al.*, Severe pre-eclampsia is associated with alterations in cytotrophoblasts of the
919 smooth chorion. *Development* **144**, 767-777 (2017).
920 105. R. Calicchio *et al.*, Preeclamptic plasma induces transcription modifications involving the AP-1
921 transcriptional regulator JDP2 in endothelial cells. *Am J Pathol* **183**, 1993-2006 (2013).
922 106. W. Fan *et al.*, Upregulation of METTL14 contributes to trophoblast dysfunction by elevating FOXO3a
923 expression in an m(6)A-dependent manner. *Placenta* **124**, 18-27 (2022).
924 107. J. Wang, F. Gao, X. Zhao, Y. Cai, H. Jin, Integrated analysis of the transcriptome-wide m6A methylome in
925 preeclampsia and healthy control placentas. *PeerJ* **8**, e9880 (2020).
926 108. M. Diaz *et al.*, Placental and Cord Blood Methylation of Genes Involved in Energy Homeostasis:
927 Association With Fetal Growth and Neonatal Body Composition. *Diabetes* **66**, 779-784 (2017).
928 109. P. Murthi, G. Rajaraman, J. Erwich, E. Dimitriadis, Decreased Placental FPR2 in Early Pregnancies That
929 Later Developed Small-For-Gestation Age: A Potential Role of FPR2 in the Regulation of Epithelial-
930 Mesenchymal Transition. *Cells* **9**, (2020).
931 110. A. Chu *et al.*, Aldehyde dehydrogenase isoforms and inflammatory cell populations are differentially
932 expressed in term human placentas affected by intrauterine growth restriction. *Placenta* **81**, 9-17 (2019).
933 111. A. Dobierzewska *et al.*, Impairment of Angiogenic Sphingosine Kinase-1/Sphingosine-1-Phosphate
934 Receptors Pathway in Preeclampsia. *PLoS One* **11**, e0157221 (2016).
935 112. M. H. Fenstad *et al.*, Genetic and molecular functional characterization of variants within TNFSF13B, a
936 positional candidate preeclampsia susceptibility gene on 13q. *PLoS One* **5**, (2010).

937 113. J. G. Grudzinskas *et al.*, Identification of high-risk pregnancy by the routine measurement of pregnancy-
938 specific beta 1-glycoprotein. *Am J Obstet Gynecol* **147**, 10-12 (1983).
939 114. K. Pihl, T. Larsen, I. Laursen, L. Krebs, M. Christiansen, First trimester maternal serum pregnancy-specific
940 beta-1-glycoprotein (SP1) as a marker of adverse pregnancy outcome. *Prenat Diagn* **29**, 1256-1261 (2009).
941 115. R. M. Silver, K. D. Heyborne, K. K. Leslie, Pregnancy specific beta 1 glycoprotein (SP-1) in maternal
942 serum and amniotic fluid; pre-eclampsia, small for gestational age fetus and fetal distress. *Placenta* **14**,
943 583-589 (1993).
944 116. M. A. Mohamad *et al.*, A Review of Candidate Genes and Pathways in Preeclampsia-An Integrated
945 Bioinformatical Analysis. *Biology (Basel)* **9**, (2020).
946 117. B. Vora *et al.*, Meta-Analysis of Maternal and Fetal Transcriptomic Data Elucidates the Role of Adaptive
947 and Innate Immunity in Preterm Birth. *Front Immunol* **9**, 993 (2018).
948 118. M. N. Moufarrej *et al.*, Early prediction of preeclampsia in pregnancy with cell-free RNA. *Nature* **602**,
949 689-694 (2022).
950 119. J. Shang, L. Lin, X. Huang, L. Zhou, Q. Huang, Re-expression of circ_0043610 contributes to trophoblast
951 dysfunction through the miR-558/RYBP pathway in preeclampsia. *Endocr J* **69**, 1373-1385 (2022).
952 120. Y. Zhang, S. Fang, J. Wang, S. Chen, R. Xuan, Hsa_circ_0008726 regulates the proliferation, migration,
953 and invasion of trophoblast cells in preeclampsia through modulating the miR-1290-LHX6 signaling
954 pathway. *J Clin Lab Anal* **36**, e24540 (2022).
955 121. J. Wang *et al.*, Alpha-2-macroglobulin is involved in the occurrence of early-onset pre-eclampsia via its
956 negative impact on uterine spiral artery remodeling and placental angiogenesis. *BMC Med* **21**, 90 (2023).
957 122. J. A. Tronco *et al.*, Alpha-2-macroglobulin from circulating exosome-like vesicles is increased in women
958 with preterm pregnancies. *Sci Rep* **10**, 16961 (2020).
959 123. K. Leavey, S. L. Wilson, S. A. Bainbridge, W. P. Robinson, B. J. Cox, Epigenetic regulation of placental
960 gene expression in transcriptional subtypes of preeclampsia. *Clin Epigenetics* **10**, 28 (2018).
961 124. R. K. Yuen, M. S. Penaherrera, P. von Dadelszen, D. E. McFadden, W. P. Robinson, DNA methylation
962 profiling of human placentas reveals promoter hypomethylation of multiple genes in early-onset
963 preeclampsia. *Eur J Hum Genet* **18**, 1006-1012 (2010).

964 125. J. Pan, X. Tian, H. Huang, N. Zhong, Proteomic Study of Fetal Membrane: Inflammation-Triggered
965 Proteolysis of Extracellular Matrix May Present a Pathogenic Pathway for Spontaneous Preterm Birth.
966 *Front Physiol* **11**, 800 (2020).
967 126. T. Lekva *et al.*, Dysregulated non-coding telomerase RNA component and associated exonuclease XRN1
968 in leucocytes from women developing preeclampsia-possible link to enhanced senescence. *Sci Rep* **11**,
969 19735 (2021).
970 127. W. Lai, L. Yu, Elevated MicroRNA 183 Impairs Trophoblast Migration and Invasiveness by
971 Downregulating FOXP1 Expression and Elevating GNG7 Expression during Preeclampsia. *Mol Cell Biol*
972 **41**, (2020).
973 128. J. Chen *et al.*, Silencing of long non-coding RNA NEAT1 improves Treg/Th17 imbalance in preeclampsia
974 via the miR-485-5p/AIM2 axis. *Bioengineered* **12**, 8768-8777 (2021).
975 129. S. Gremlich *et al.*, The long non-coding RNA NEAT1 is increased in IUGR placentas, leading to potential
976 new hypotheses of IUGR origin/development. *Placenta* **35**, 44-49 (2014).
977 130. J. Schuster *et al.*, Protein Network Analysis of Whole Exome Sequencing of Severe Preeclampsia. *Front*
978 *Genet* **12**, 765985 (2021).
979 131. Z. Miao, M. Chen, H. Wu, H. Ding, Z. Shi, Comparative proteomic profile of the human placenta in normal
980 and fetal growth restriction subjects. *Cell Physiol Biochem* **34**, 1701-1710 (2014).
981 132. J. Zhao *et al.*, The m(6)A methyltransferase METTL3 promotes trophoblast cell invasion by regulating
982 MYLK expression. *Placenta* **129**, 1-6 (2022).
983 133. J. Zadora *et al.*, Disturbed Placental Imprinting in Preeclampsia Leads to Altered Expression of DLX5, a
984 Human-Specific Early Trophoblast Marker. *Circulation* **136**, 1824-1839 (2017).
985 134. H. Tiensuu *et al.*, Human placental proteomics and exon variant studies link AAT/SERPINA1 with
986 spontaneous preterm birth. *BMC Med* **20**, 141 (2022).
987 135. F. Zhou, T. Cheng, Y. Xing, H. Ma, L. Yang, Network exploration of gene signatures underlying low birth
988 weight induced metabolic alterations. *Medicine (Baltimore)* **101**, e31489 (2022).
989 136. M. A. Deyssenroth *et al.*, Whole-transcriptome analysis delineates the human placenta gene network and its
990 associations with fetal growth. *BMC Genomics* **18**, 520 (2017).

991 137. D. A. Enquobahrie, C. Qiu, S. Y. Muhie, M. A. Williams, Maternal peripheral blood gene expression in
992 early pregnancy and preeclampsia. *Int J Mol Epidemiol Genet* **2**, 78-94 (2011).
993 138. A. K. Edwards, K. A. Dunlap, T. E. Spencer, M. C. Satterfield, Identification of Pathways Associated with
994 Placental Adaptation to Maternal Nutrient Restriction in Sheep. *Genes (Basel)* **11**, (2020).
995